



## **AFFIDAVIT**

I declare that I have authored this thesis independently, that I have not used other than the declared sources/resources, and that I have explicitly indicated all material which has been quoted either literally or by content from the sources used. The text document uploaded to TUGRAZonline is identical to the present master's thesis.

---

Date

---

Signature

# Abstract

The aim of this thesis is the separation of 7-dehydrocholesterol (7DHC) and vitamin D<sub>3</sub> via crystallization. Vitamin D<sub>3</sub> (VD3), which is also known as "sunshine vitamin", is a very important nutrient. A deficiency has negative effects on teeth, skeletal by subsequent osteoporosis, contributes to the development of various malignant tumors, diabetes mellitus type II, arterial hypertension, etc. [1]. Industrially, it is produced by exposing 7DHC to UV light, followed by a 2-step purification process to obtain first the unreacted 7DHC and afterwards VD3 in an amorphous state, which is referred as resin in the literature [2]. This resin has to be purified by chemical complexation, column chromatography or crystallization to obtain the purity of the united states pharmacopoeia (USP) product. In this work the separation by means of crystallization was investigated in order to obtain VD3 directly after synthesis in a crystalline state.

After carrying out several experiments, a three-step process is proposed which includes the separation of 7DHC and results in crystalline VD3. The proposed process can be operated in continuous mode. Furthermore, no temperatures above 30°C were used in the process. As a result, unintended side reactions and decomposition of the vitamin can be prevented. In step 1, a solvent switch takes place and most of the 7DHC can be separated and re-used in the upstream synthesis. Step 1 is particularly important because the photochemical synthesis has only a conversion of 20-30% and a large amount of 7DHC has to be separated. Next, step 2 is a purification step where almost all of the 7DHC is separated. Either anti-solvent or cooling crystallization was shown to be possible for this step. The crystal mixture of this step could be recycled back into step 1. Finally step three is the crystallization of VD3. Here a temperature controlled anti-solvent crystallization could be carried out to control polymorphism of VD3.

To develop this process, solubility data of 7DHC and VD3 were first obtained. Subsequently, experiments were conducted in a so-called mixed suspension mixed product removal reactor (MSMPR) to obtain crystallization data as well as the behavior of the two substances in continuous operation mode. In these experiments, resin formation and deposition in the crystallizer occurred. Resin formation was investigated further and could be avoided with the help of the findings from polymorphism experiments.

Based on the obtained solubility data, batch experiments were carried out to investigate the separation of VD3 and 7DHC by cooling and anti-solvent crystallization. The starting point of the experiments was a mixture equal to a solution after photochemical synthesis with a conversion of 30%. More than 98% of the 7DHC was removed from the solution within the first two separation steps. This high separation was probably possible through co-crystallization of 7DHC with the vitamin and led to concentrations far below the obtained solubility of 7DHC. The remaining filtrate after the second separation step consists mostly of VD3 and was subsequently crystallized with a continuous anti-solvent crystallization in an MSMPR as final process step.

# Kurzfassung

Ziel dieser Arbeit ist die Trennung von 7-Dehydrocholesterol (7DHC) und Vitamin D<sub>3</sub> mittels Kristallisation. Vitamin D<sub>3</sub> (VD<sub>3</sub>), welches auch als "Sonnenschein Vitamin" bekannt ist, ist ein sehr wichtiger Nährstoff. Ein Mangel hat negative Auswirkungen auf die Zähne, Skelett durch nachfolgende Osteoporose, trägt zur Entwicklung von verschiedenen bösartigen Tumoren bei, verursacht Diabetes mellitus Typ II, arterielle Hypertonie, etc. [1]. Industriell wird es hergestellt, indem man 7DHC UV-Licht aussetzt, gefolgt von einem 2-stufigen Reinigungsverfahren um zuerst das nicht umgesetzte 7DHC und danach VD<sub>3</sub> in einem amorphen Zustand zu erhalten, welcher in der Literatur als "Resin" bezeichnet wird [2]. Dieses Resin muss durch chemische Komplexbildung, Säulenchromatographie oder Kristallisation gereinigt werden, um das USP-Produkt (United States Pharmacopoeia) zu erhalten. In dieser Arbeit wurde die Trennung mittels Kristallisation untersucht, um VD<sub>3</sub> direkt nach der Synthese im kristallinen Zustand zu erhalten.

Es wurde ein dreistufiger Prozess entwickelt, welcher die Trennung von 7DHC einschließt und zu kristallinen VD<sub>3</sub> führt. Der vorgeschlagene Prozess kann kontinuierlich betrieben werden. Weiterhin wurden im Prozess keine Temperaturen über 30°C eingesetzt. Infolgedessen sollten unbeabsichtigte Neben- und Zersetzungsreaktionen des Vitamins verhindert werden. In Schritt 1 findet ein Lösungsmittelwechsel statt und der Großteil des 7DHC kann abgetrennt und in der Synthese wiederverwendet werden. Schritt 1 ist besonders wichtig, da die photochemische Synthese nur eine Umwandlung von 20-30% aufweist und eine große Menge an 7DHC abgetrennt werden muss. Der nächste Schritt ist ein Reinigungsschritt, wobei fast das gesamte 7DHC abgetrennt wird. Es wurde gezeigt, dass entweder eine Antisolvent- oder Kühlungskristallisation möglich ist. Die Kristallmischung dieses Schrittes könnte wieder in Schritt 1 zurückgeführt werden. Anschließend kommt Schritt 3 als Kristallisationsschritt von VD<sub>3</sub>. Hier konnte eine Antisolvent-Kristallisation durchgeführt werden, um den temperaturabhängigen Polymorphismus von VD<sub>3</sub> zu kontrollieren.

Um diesen Prozess zu entwickeln, wurden zuerst Löslichkeitsversuche von 7DHC und VD<sub>3</sub> durchgeführt. Anschließend wurden Experimente in einem sogenannten MSMPR (mixed suspension mixed product removal reactor) durchgeführt, um sowohl Kristallisationsdaten als auch das Verhalten der beiden Substanzen im kontinuierlichen Betrieb zu erhalten. In diesen Experimenten trat eine Resinbildung sowie Abscheidungen im Kristallisator auf. Die Resinbildung wurde im Weiteren untersucht und konnte mit Hilfe der Ergebnisse aus den Polymorphie-Experimenten vermieden werden.

Basierend auf den erhaltenen Löslichkeitsdaten wurden Batch-Experimente durchgeführt, um die Trennung von VD<sub>3</sub> und 7DHC durch Kühlungs- und Antisolvent-Kristallisation zu untersuchen. Ausgangspunkt der Experimente war eine Mischung mit einer Umwandlung von 30%, entsprechend einer Lösung nach der



photochemischen Synthese. Mehr als 98% des 7DHC wurden aus der Lösung innerhalb der ersten beiden Trennschritte entfernt. Diese hohe Trennung war vermutlich durch Co-Kristallisation von 7DHC mit dem Vitamin möglich und führte zu Konzentrationen weit unterhalb der erhaltenen Löslichkeit von 7DHC. Das verbleibende Filtrat nach dem zweiten Trennschritt bestand größtenteils aus VD3 und wurde anschließend mit einer kontinuierlichen Antisolvent-Kristallisation in einem MSMPR als abschließenden Prozessschritt kristallisiert.

# Acknowledgement

First I would like to thank my thesis adviser Heidrun Gruber-Wölfler for the excellent support of my work as well as the possibility to be part of her research team at the Institute of Process and Particle Engineering. Furthermore, I would like to thank the laboratory team for the many helpful and amusing hours in and outside the laboratory.

I would like to thank the team of Volker Hessel at Eindhoven University of Technology Micro Flow Chemistry and Process Technology Department Chemical Engineering and Chemistry, especially Marc Escribà-Gelonch for co-operation and useful remarks during my work.

Finally, I would like to thank my girlfriend, brother and parents for providing me with support and encouragement throughout my years of study. This accomplishment would not have been possible without them. Thank you

# Contents

<b>List of Figures</b>	<b>9</b>
<b>List of Tables</b>	<b>11</b>
<b>1 Introduction</b>	<b>12</b>
1.1 Vitamin D <sub>3</sub> . . . . .	12
1.1.1 Vitamin D <sub>3</sub> synthesis . . . . .	12
1.1.2 Vitamin D <sub>3</sub> polymorphism . . . . .	13
1.2 Industrial process . . . . .	15
1.3 Objective and motivation . . . . .	16
<b>2 Crystallization basics</b>	<b>17</b>
2.1 Driving force . . . . .	17
2.2 Nucleation . . . . .	18
2.2.1 Primary nucleation . . . . .	19
2.2.2 Secondary nucleation . . . . .	22
2.3 Crystal growth . . . . .	22
2.4 MSMPR crystallizer . . . . .	23
2.4.1 Derivation utilizing population density . . . . .	23
2.4.2 Population density from size distribution . . . . .	26
2.4.3 Growth and nucleation kinetics . . . . .	27
<b>3 Results and Discussion</b>	<b>28</b>
3.1 Solubility of commercial VD3 in ACN . . . . .	28
3.2 MSMPR experiments VD3 . . . . .	30
3.3 VD3 resin . . . . .	33
3.4 VD3 polymorphism experiments . . . . .	35
3.4.1 VD3 crystal formation and growth in ACN . . . . .	36
3.4.2 Solubility of VD3 form B in ACN . . . . .	38
3.5 Solubility 7DHC in ACN . . . . .	41
3.6 MSMPR experiments with 7DHC . . . . .	42
3.7 Separation Process . . . . .	44
3.7.1 Batch experiments . . . . .	44
3.7.2 Antisolvent batch experiments . . . . .	47
3.7.3 Antisolvent MSMPR experiment . . . . .	48
3.7.4 Proposed separation process . . . . .	52
<b>4 Summary</b>	<b>54</b>

---

<b>5 Outlook</b>	<b>57</b>
<b>6 Methods and Materials</b>	<b>58</b>
6.1 High pressure liquid chromatography - HPLC . . . . .	58
6.1.1 HPLC calibration . . . . .	58
6.2 Pumps . . . . .	61
6.3 Magnetic stirrer . . . . .	61
6.4 Ultrasonic bath . . . . .	61
6.5 Thermostat - Heater/Cooler . . . . .	61
6.6 Vacuum pump and rotary evaporator . . . . .	61
6.7 Microscope . . . . .	61
6.8 Helos . . . . .	61
6.9 Raman . . . . .	62
6.10 Sampling from suspensions . . . . .	62
6.11 Used chemicals . . . . .	62
<b>7 Appendix</b>	<b>63</b>
7.1 Glossary . . . . .	63
<b>Bibliography</b>	<b>64</b>

# List of Figures

1.1	VD3 Synthesis [11, 5] . . . . .	13
1.2	Conformation conformers of VD3 and crystal structure of form A [12] . .	14
1.3	XRD spectra of different VD3 samples. Left: data from Mei [12]. Right: data from our group [16] <b>a</b> : commercial VD3, <b>b</b> : example of a sample of VD3 with form A, <b>c</b> : example of a sample with form B . . . . .	14
1.4	Raman spectra of different VD3 samples [16]: <b>a</b> : commercial VD3, <b>b</b> : example of a sample of VD3 with form A, <b>c</b> : example of a sample with form B . . . . .	15
1.5	Flow diagram of the industrial production of VD3 [5] . . . . .	16
2.1	Solubility regions as function of concentration and temperature [20] . . .	18
2.2	Nucleation types [22] . . . . .	19
2.3	Free energy versus the size of nuclei showing a critical nuclei size [22]. Smaller Particles than $r_c$ tend to dissolve again and bigger particles will continue to grow . . . . .	20
2.4	Wetting angle $\phi$ shown by the interfacial tensions at the boundaries between two solid phases and one liquid phase [22] . . . . .	22
2.5	MSMPR crystallizer concept . . . . .	24
2.6	MSMPR crystallizer formalism shown in a semilogarithmic population density versus size plot [26] . . . . .	25
2.7	Types of semi-logarithmic population density plots and potential causes [26] . . . . .	26
3.1	Obtained solubility data of VD3 in ACN compared to the literature [27] .	29
3.2	Experimental MSMPR setup for the continuous crystallization of VD3 in ACN . . . . .	30
3.3	VD3 crystals prepared in MSMPR experiment 5 . . . . .	32
3.4	MSMPR evaluation of the population density of experiment 5 with a selected cut size of $28 \mu\text{m}$ . . . . .	33
3.5	VD3 crystals obtained by re-crystallization of the commercial VD3 at $-20^\circ\text{C}$ in ACN . . . . .	34
3.6	Commercial VD3 crystals directly measured . . . . .	35
3.7	Raman spectra of VD3 <b>a</b> : commercial, <b>b</b> : form B from the experiment .	36
3.8	Free growing VD3 crystals on the microscope slide by slow evaporation of ACN . . . . .	37
3.9	Agglomerated VD3 crystals in suspension obtained by re-crystallization of commercial VD3 at $-20^\circ\text{C}$ . . . . .	38

3.10	Solubility of the different polymorphic forms of VD3 in ACN . . . . .	39
3.11	Raman spectra: <b>a</b> commercial VD3, <b>b</b> sample crystallized at 10°C, <b>c</b> sample crystallized at -10°C, <b>d</b> sample crystallized at -20°C . . . . .	39
3.12	Zoom of the front part of the HPLC chromatogram of commercial VD3 and VD3 directly measured after 300 minutes at 10 and 25°C in ACN to show possible reactions . . . . .	40
3.13	Solubility data of VD3 and 7DHC in ACN . . . . .	41
3.14	Crystal growth rate over supersaturation . . . . .	43
3.15	Fit crystals growth rate . . . . .	43
3.16	Batch steps for experiment one to three . . . . .	45
3.17	Concentrations in the filtrate of experiment 4 after separation 1 and 2 at 25 and -20°C, respectively . . . . .	46
3.18	Obtained crystals of experiment 1 . . . . .	47
3.19	Separation of VD3 and 7DHC in ACN with water as anti-solvent at 25°C . . . . .	48
3.20	MSMPR anti-solvent setup for the continuous crystallization of VD3 . . . . .	49
3.21	Density distribution step 3 . . . . .	49
3.22	VD3 product crystals of step 3 suspended with a surfactant in water . . . . .	50
3.23	Raman spectra of step 3 product . . . . .	51
3.24	MSMPR evaluation of the semilogarithmic population density of step 3 with a selected cut size of 6.25 $\mu\text{m}$ . . . . .	51
3.25	Proposed 3 step process to separate VD3 and 7DHC. Step 1: Solvent switch to ACN because of the high solubility of the used ether to separate most of the 7DHC. Step 2: Further purification were almost all of the 7DHC is separated. Either anti-solvent or cooling crystallization could be possible. Step 3: Temperature controlled anti-solvent crystallization of VD3 to control polymorphism . . . . .	53
6.1	HPLC calibration of VD3. Area versus concentration . . . . .	59
6.2	HPLC calibration of 7DHC. Area versus concentration . . . . .	60
6.3	HPLC calibration of E321. Area versus concentration . . . . .	60

# List of Tables

3.1	Process conditions of the MSMPR experiments with VD3 in ACN . . . .	31
3.2	MSMPR experiments with 7DHC in ACN . . . . .	42
3.3	Batch experiments with two separation steps . . . . .	44
6.1	Calibration VD3 . . . . .	58
6.2	Calibration 7DHC . . . . .	59
6.3	Calibration E321 . . . . .	59

# 1 Introduction

## 1.1 Vitamin D<sub>3</sub>

Vitamin D<sub>3</sub> (VD<sub>3</sub>) belongs to a group of fat-soluble steroids and is responsible for the absorption of calcium and phosphorus, cell growth and renewal, hormonal regulation of the immune system, as well as other body processes. An optimal supply of this vitamin is of crucial importance for the health of children, adults and the elderly. A deficiency of vitamin D has negative effects on teeth, skeletal by subsequent osteoporosis, contributes to the development of various malignant tumors, primarily in the colon, the prostate and breast, as well as autoimmune and allergic diseases, diabetes mellitus type II, arterial hypertension, etc [1].

The first commercial production of vitamin D<sub>3</sub> was achieved in 1936 by Adolph Windaus et al. [3]. In his work he isolated 7-dehydrocholesterol from pig skin, characterized the molecule and produced vitamin D<sub>3</sub> by UV irradiation of the 7-dehydrocholesterol (7DHC). In the same year Elliot et al. [4] showed that crystalline vitamin D<sub>3</sub> added to milk at 400 USP units was more effective than cod liver oil, which was used as the major source against rickets, in both human and animal nutrition.

Vitamin D<sub>3</sub> production today [5] starts with the isolation of cholesterol. Cholesterol can be extracted from almost all animals spinal cords and brains. However, the commercial major source is from sheep's wool, because of the danger of co-extracting harmful proteins. By washing the sheep's wool, wool grease is obtained as a by-product. The grease contains about 15% cholesterol and is a mixture of long-chain fatty-acid esters. Saponification of the grease gives fatty acid soaps and wool grease alcohols. The latter contains the cholesterol and a mixture of other sterols and fatty alcohols. Next, the acid soaps are separated by filtration. Finally, Cholesterol is obtained by complexation with calcium or magnesium chloride from the wool grease alcohols and crystallization of the broken complex with methanol.

### 1.1.1 Vitamin D<sub>3</sub> synthesis

Synthesis steps of vitamin D<sub>3</sub> are shown in figure 1.1. First cholesterol is converted within four chemical process steps to 7-dehydrocholesterol [6, 7]. This procedure by Windaus and Schenk has been recently improved [8, 9] to be the majority of 7-dehydrocholesterol production. Next, provitamin 7DHC is photochemical irradiated to form the pre vitamin D. The optimum wavelength of light for the conversion to pre vitamin D was theoretical calculated and confirmed experimentally to be 296 nm [10]. Pre vitamin undergoes a thermal equilibrium to form the *cis* vitamin which is the commercial available vitamin



D<sub>3</sub>. Both pre and *cis* vitamin are considered as the active form of vitamin D<sub>3</sub>. The equilibrium composition is at approximately 80% vitamin D<sub>3</sub> by heating the vitamin at 60 - 80°C for several hours. The pre isomer equilibrates to form 80% *cis* at -20°C in 2204 days and at 20°C in 13 days [5]. Furthermore, pre vitamin D can undergo photoisomerization to undesired by-products. Irradiation with UV-light leads to equilibrium mixtures of tachysterol, lumisterol as well as back reactions to 7-dehydrocholesterol, depending on the used wavelength of light, temperature and time.

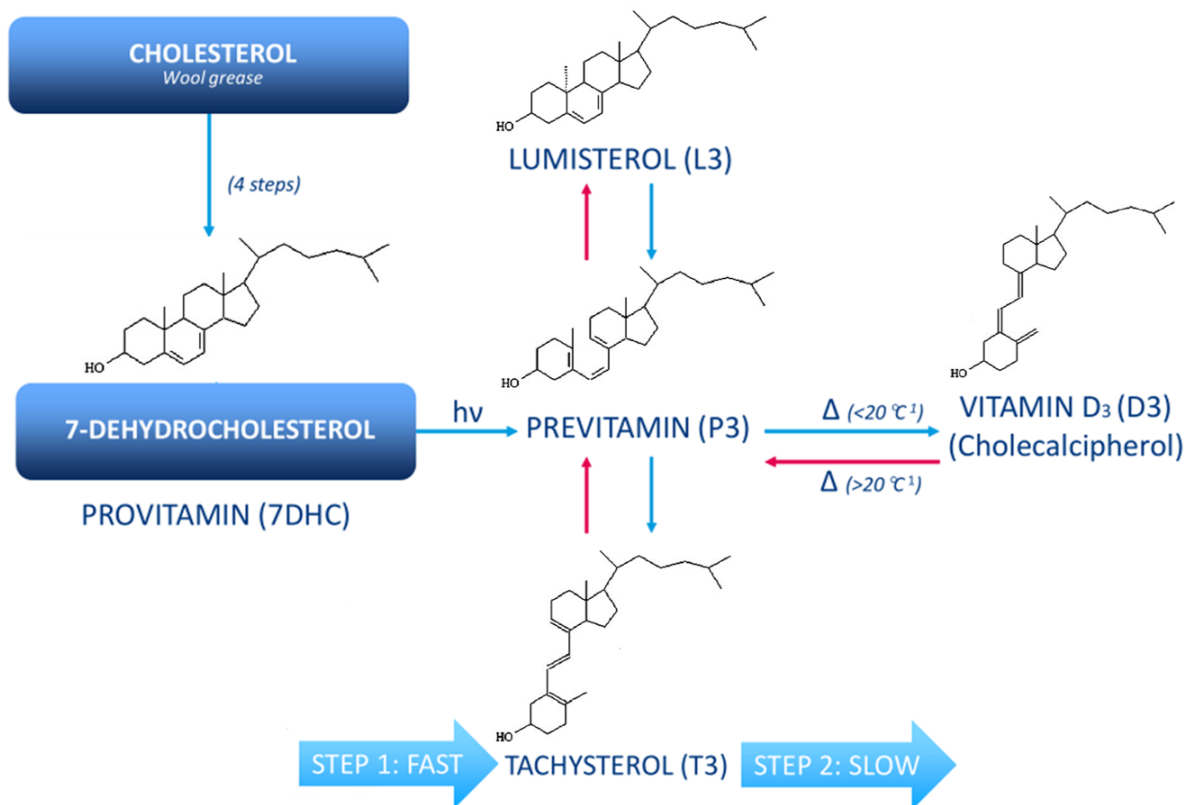


Figure 1.1: VD<sub>3</sub> Synthesis [11, 5]

### 1.1.2 Vitamin D<sub>3</sub> polymorphism

Two polymorphic forms of crystalline vitamin D<sub>3</sub> were recently reported by Mei et al. [12]. Crystalline orthorhombic form A exists as a homodimer of a 1:1 complex of  $\alpha$ - and  $\beta$ - A ring chairs, figure 1.2. The more unstable polymorph B only consists of the  $\alpha$  conformer. In his work, Mei was recrystallizing the commercial available form A in a variety of procedures and solvent selections, as described in [2]. A glassy transparent film, corresponding to an amorphous state of vitamin D<sub>3</sub>, was obtained in most of the crystallization experiments conducted under ambient conditions. This amorphous state is referred to as vitamin D<sub>3</sub> resin in the literature. By recrystallization from a saturated acetonitrile (ACN) solution at temperatures below 5°C, form B and concomitant form

A crystals were obtained. In further studies, pure crystalline form B was prepared repeatedly by maintaining temperatures below  $-20^{\circ}\text{C}$  with alcohols as solvent.

Mei associated the  $\alpha$  conformer as the root cause of the VD3 instability. In solution, VD3 exists as a dynamically equilibration mixture of  $\alpha$  and  $\beta$  conformers. Their ratio was reported to be temperature and solvent dependent [13, 14, 15]. The  $\alpha$  ratio increases as the polarity of the solvent increases and the temperature decreases.

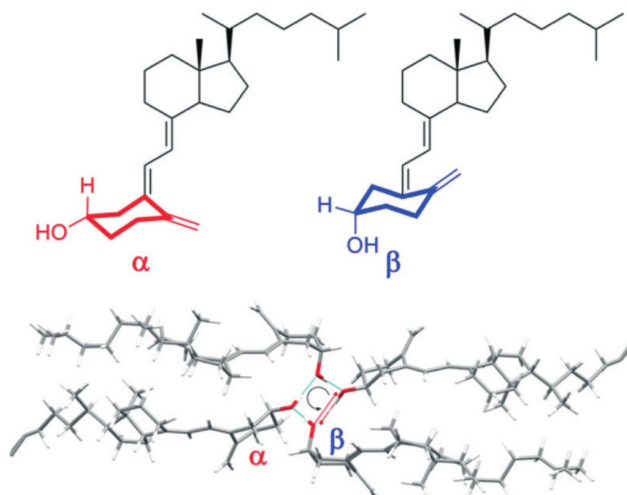


Figure 1.2: Conformation conformers of VD3 and crystal structure of form A [12]

Identification of the VD3 polymorphs can be done by XRD, DSC, NMR, Raman spectroscopy and other methods [12]. In this work Raman spectroscopy will be used for the distinction of the polymorphs. In order to be consistent with the work of Mei, different polymorphs were measured with XRD, identified and then measured again with Raman spectroscopy [16]. The comparison can be seen in figure 1.3. An example of the significant zones of Raman spectra of commercial VD3, VD3 in form A and B is given in figure 1.4. Differences in the spectra of form A and B were shown at approximately  $2950\text{ cm}^{-1}$ ,  $960\text{ cm}^{-1}$  and  $720\text{ cm}^{-1}$ .

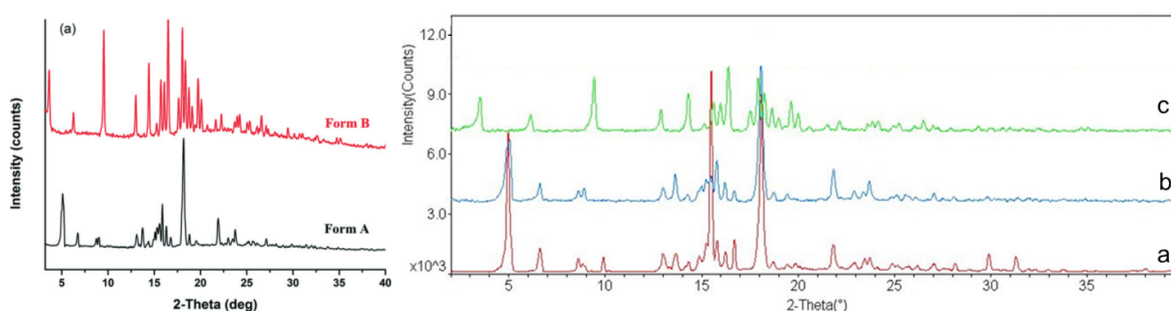


Figure 1.3: XRD spectra of different VD3 samples. Left: data from Mei [12]. Right: data from our group [16] **a**: commercial VD3, **b**: example of a sample of VD3 with form A, **c**: example of a sample with form B

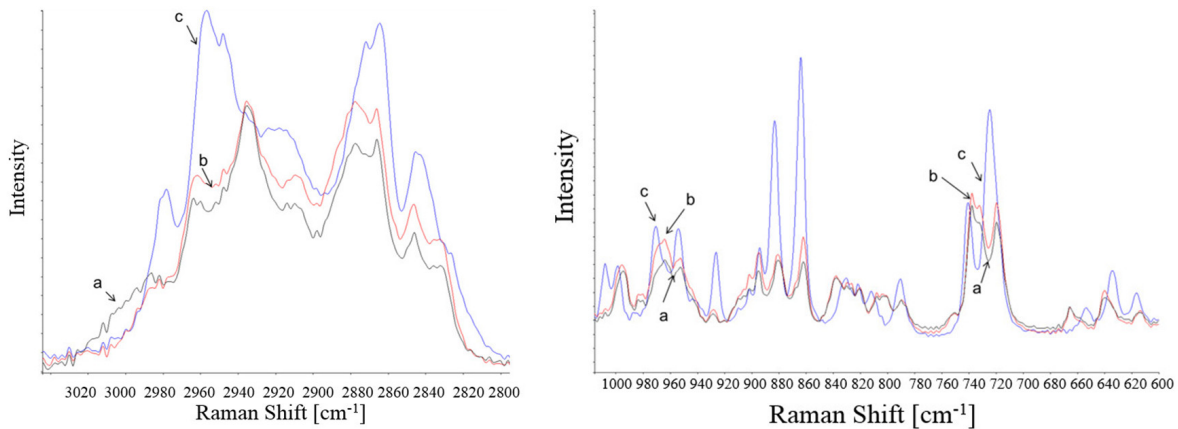


Figure 1.4: Raman spectra of different VD3 samples [16]: **a**: commercial VD3, **b**: example of a sample of VD3 with form A, **c**: example of a sample with form B

## 1.2 Industrial process

Industrially, vitamin D<sub>3</sub> is produced by irradiation of 7-dehydrocholesterol and four subsequent purification steps, as shown in figure 1.5 [5]. The synthesis process mimics the processes in the body. 7DHC is dissolved in an appropriate solvent, e.g. peroxid-free diethyl ether, and then irradiated in a reactor similar to the human skin. The cooled solution is pumped through a UV-transparent quartz reactor, irradiated with UV-light from high-pressure mercury lamps and circulated until a conversion of 20-30% is achieved. In the resulting solution a mixture of 7DHC, pre vitamin D, vitamin D and irradiation by-products can be found. Irradiation must be performed under conditions that favor the production of pre vitamin. Mercury lamps are the most used UV light sources. However, higher yields with a more favorable isomer distribution can be achieved with light kept at 275-300 nm and an optimum at 295 nm as mentioned above. After the desired conversion is achieved, the solution is stabilized against oxidation by the addition of  $\leq 1$  wt% butylated hydroxyanisole or butylated hydroxytoluene (E321).

In the first purification step a discontinuous solvent swap takes place. Ether is evaporated for reuse and substituted with an alcohol, e.g., methanol. Next 7DHC is separated through this solvent swap by precipitation and let to crystallize in the next tank. 7DHC is recovered by filtration and reused in subsequent irradiations. The remaining solution is then evaporated under vacuum and the residual oil is heated to isomerize pre to *cis* vitamin D. Vitamin D obtained from this process is a pale yellow-to-amber oil that flows freely when hot and becomes brittle when cold. In the final step the resin needs to be purified to give the USP product. This can be done by chemical complexation, column chromatography or crystallization. Crystalline VD3 can be obtained by crystallizing the resin with a mixture of hydrocarbon solvents and aliphatic nitriles, e.g., benzene and acetonitrile [17, 18]. The total yield of the current industrial process for the production of VD3 is less than 20% [19]. Main producers of this vitamin are the companies DSM

(NL), Hoffman La Roche (CHE) and BASF (GER).

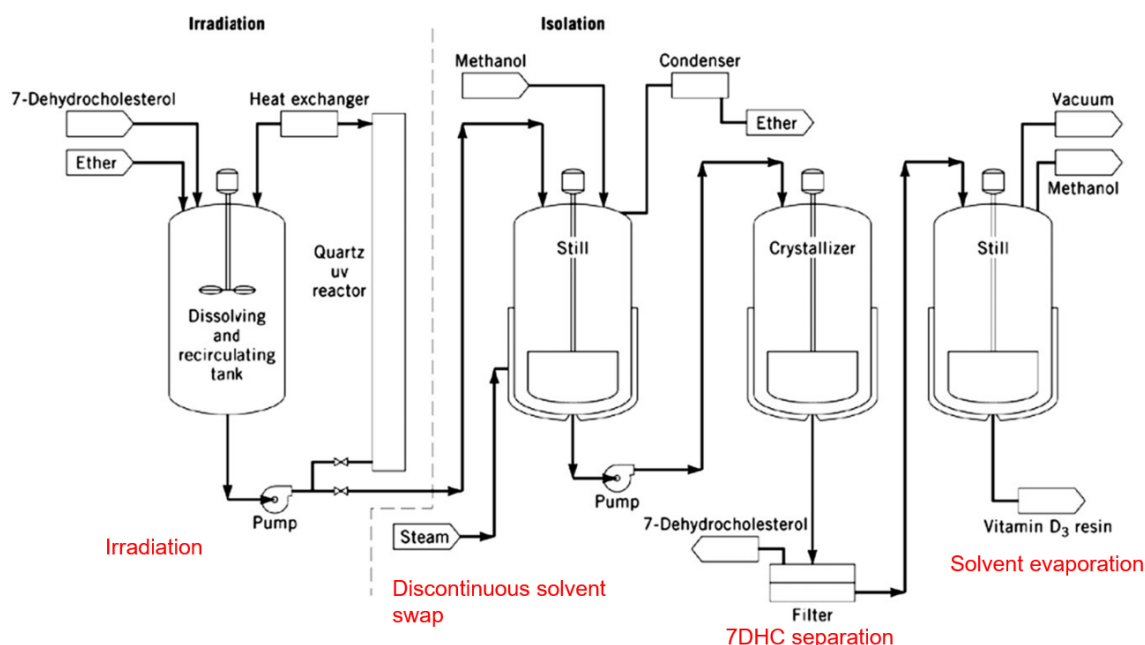


Figure 1.5: Flow diagram of the industrial production of VD3 [5]

### 1.3 Objective and motivation

This work was realized within the research groups of H. Gruber-Wölfler<sup>1</sup> and V. Hessel<sup>2</sup> and contributes to the funding awarded by Marc Escrivà-Gelonch<sup>2</sup> by the Horizon 2020: Marie Skłodowska-Curie Individual Fellowship under grant agreement number 659233.

The goal of the group is to develop a continuous vitamin D<sub>3</sub> production process, starting with its continuous synthesis up to the final purification via crystallization in flow. Starting point of this work is after the continuous synthesis of vitamin D<sub>3</sub> in tert-butyl methyl ether (tBME). Aim of this work is to develop an efficient crystallization process which enables the separation of 7DHC and VD3. It is intended to create a transition to the continuous crystallization of VD3 in ACN. Furthermore, the current industrial separation process should be used as a guidance in the separation process development and may be improved. Various operation conditions and crystallization techniques are tested in order to obtain crystalline VD3 with high yield and purity. Therefore, it is important to deal in the following with the basics of crystallization.

<sup>1</sup>Graz University of Technology Institute of Process and Particle Engineering

<sup>2</sup>Eindhoven University of Technology Micro Flow Chemistry and Process Technology Department Chemical Engineering and Chemistry

## 2 Crystallization basics

Crystallization is a powerful thermal unit operation and can be used for separation of multi-component mixtures. Depending on the desired product, the goal of crystallization can be either to obtain crystals, a solution with high purity or to gain as much of the desired component as possible out of the system. As system a multi-component mixture in solid, gaseous or liquid state is defined. Furthermore, the system can be divided into mixtures without additives e.g. melt crystallization or with additives e.g. solvent crystallization.

Next, crystallization can be categorized according to the driving force. This driving force is the difference between the saturated and the supersaturated state of the system. The achievement of this supersaturated state can be done, either by cooling, evaporation, evaporative cooling, by reaction of substances or by applying a high pressure. It is also possible by lowering the solubility of the desired product by the addition of another soluble substance e.g. drawing-out with salts, or with a liquid anti-solvent agent.

The crystallization process can be further divided by the type of operation in continuous and batch processes. Here, the often mentioned advantages and disadvantages of modern thermal down-stream processes are also valid. Nevertheless, it should be noted that in the industry, mainly batch crystallizations are carried out for very high and low process flow rates [20].

This work deals with the challenging task to design a continuous separation process via crystallization at low flow rates provided for example by micro or mini reactors, directly coupled after the synthesis.

### 2.1 Driving force

The driving force of the crystallization is supersaturation of the system. Supersaturation is a state where more solute is dissolved, as it may be in the thermodynamic equilibrium. The thermodynamic equilibrium of the adjacent phases can be expressed by the Gibbs equilibrium conditions [21]

$$\begin{aligned}p^\alpha &= p^\beta = \dots = p^\pi \\T^\alpha &= T^\beta = \dots = T^\pi \\ \mu^\alpha &= \mu^\beta = \dots = \mu^\pi\end{aligned}$$

whereby  $p$  represents the pressure,  $T$  the temperature and  $\mu$  the chemical potential of the respective phases  $\alpha$  and  $\beta$  in equilibrium. By changing one of these quantities in a phase to achieve a supersaturation, the system tries to restore the equilibrium state

by formation of new centers of crystallization, also known as nuclei, or by addition of excess saturated mass on existing solids. The latter is also referred to as crystal growth.

The crystallization events can take place differently depending on the type of supersaturation [20]. Figure 2.1 shows the solubility of a crystallizing component in a solvent as a function of temperature. On the bold line the system is saturated. States under this line correspond to lower concentrations than the solubility limit i.e. the system is undersaturated. Above the saturation line the system can be divided into two zones, in a metastable and supersaturated. Here, the concentration is higher than in the saturated state. When the system exceeds the dashed overcritical solubility line, a supersaturated state is reached. Here the formation of a solid phase occurs spontaneously. Within the metastable zone already existing crystals are growing depending on the applied concentration difference to the saturated state. However, in the absence of solids, the supersaturation can last for a very long time in the metastable zone. An independent nucleation is unlikely in this region by definition.

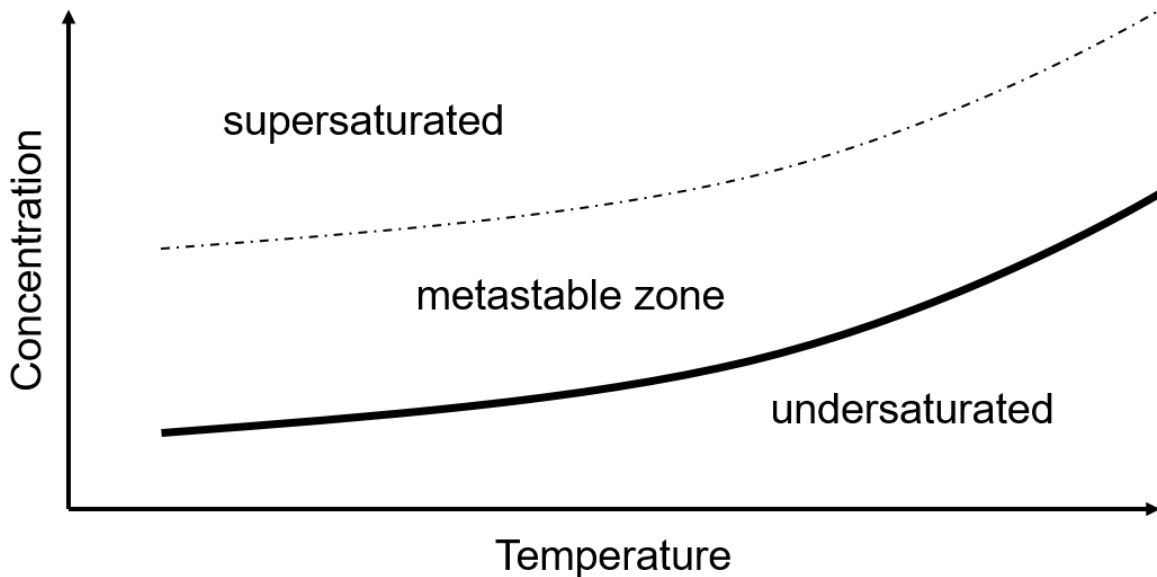


Figure 2.1: Solubility regions as function of concentration and temperature [20]

## 2.2 Nucleation

As already mentioned, an oversaturation is not enough for a system to begin to crystallize. A certain number of solid centers i.e. embryos, nuclei or seeds must exist in the solution. Nucleation may occur spontaneously in the supersaturated region otherwise it may be induced artificially. Sometimes it is hard to tell whether the system has spontaneous nucleation of its own or induced nucleation from external stimulation. Induced nucleation can be caused by agitation, mechanical shock, friction and extreme pressure

within the system. In figure 2.2 the different nucleation types are shown according to their formation.

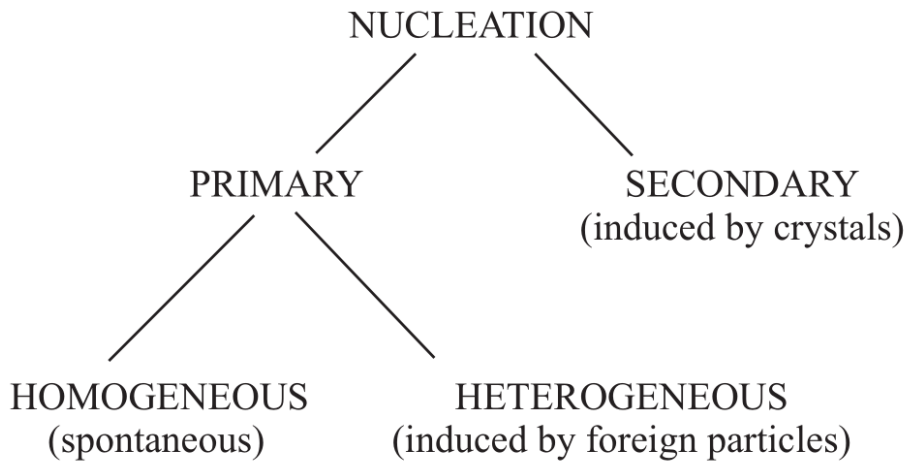


Figure 2.2: Nucleation types [22]

### 2.2.1 Primary nucleation

In this case the term primary stands for systems that do not contain crystalline matter. It can be further divided into a homogeneous nucleation, which occurs spontaneous in the supersaturated region, and heterogeneous nucleation induced by foreign particles e.g. dust particles from abrasion, cells etc.

The theory of formation and stability for **homogeneous primary nucleation** is extended for the crystallization of solids from solutions based on the condensation of a liquid from the gas phase according to changes in the Gibbs free energy [21, 23, 24]. The overall excess free energy  $\Delta G$  of a small cubic solid particle of solute and the solute in solution equals the sum of the surface excess free energy  $\Delta G_S$  and the volume excess free energy  $\Delta G_V$

$$\Delta G = \Delta G_S + \Delta G_V$$

$$\Delta G = 4\pi r^2 \gamma + \frac{4}{3}\pi r^3 \Delta G_v$$

$\Delta G_S$  is the excess free energy between the surface of the particle and the bulk of the particle and is a positive quantity with a magnitude proportional to  $r^2$ .  $\Delta G_V$  corresponds to the excess free energy between a very large particle ( $r = \infty$ ) and the solute in solution. It is for a supersaturated solution a negative quantity and proportional to  $r^3$ .  $\Delta G_v$  is the free energy change of the transformation per unit volume and  $\gamma$  is the interfacial tension between the developing crystalline surface and the supersaturated solution.

In figure 2.3 it can be seen that  $\Delta G$  passes through a maximum because of the different algebraic signs and magnitudes of  $\Delta G_S$  and  $\Delta G_V$ . The critical nuclei lies at the maximum value  $\Delta G_{\text{crit}}$  with the critical nuclei size  $r_c$ . Particles smaller than  $r_c$  tend so dissolve again and bigger particles will continue to grow.

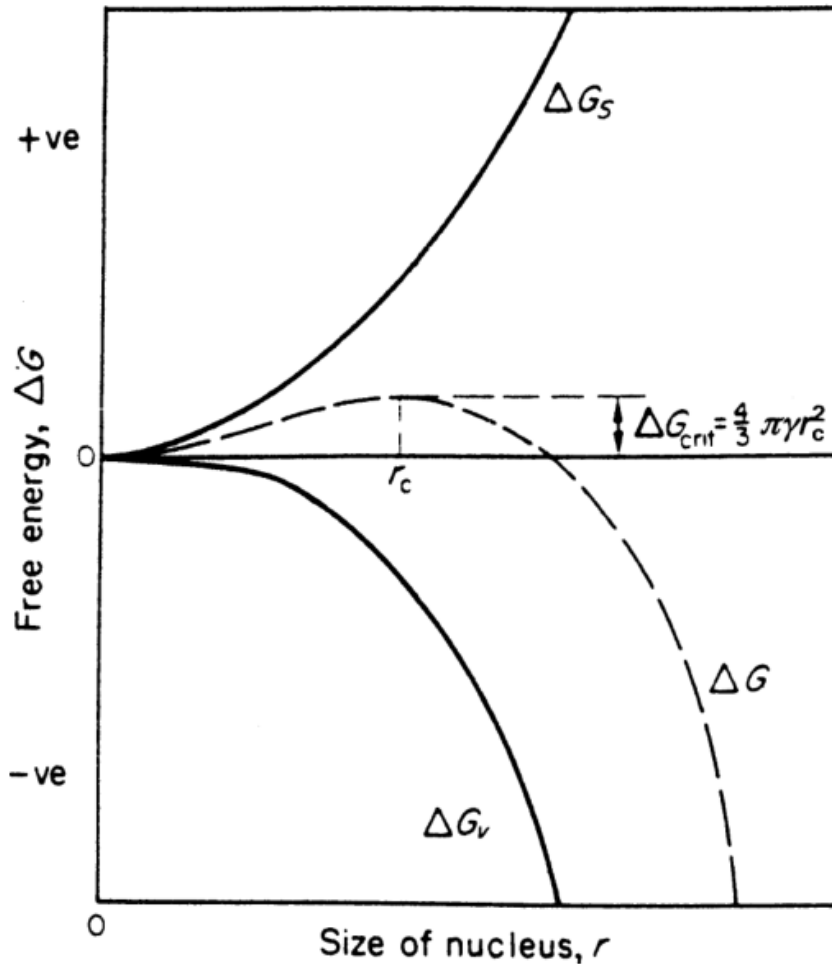


Figure 2.3: Free energy versus the size of nuclei showing a critical nuclei size [22]. Smaller Particles than  $r_c$  tend to dissolve again and bigger particles will continue to grow

The nucleation rate  $J$ , which represents the number of nuclei formed per unit of time and volume, is often written in the form of an Arrhenius approach.

$$J = Ae^{(-\frac{\Delta G}{kT})}$$

Here  $A$  is a constant value and  $k$  is the Boltzmann constant ( $1.3805 \cdot 10^{-23} JK^{-1} \text{ mol}^{-1}$ ). With the Gibbs-Thomson relation for non-electrolytes

$$\ln S = \frac{2\gamma\nu}{kTr}$$



where  $\nu$  is the molecular volume and the supersaturation ratio  $S$  defined as

$$S = \frac{c}{c^*}$$

with  $c$  as the concentration of a solute and  $c^*$  the saturated concentration of this solute; this gives

$$-\Delta G_v = \frac{2\gamma}{r} = \frac{kT \ln S}{\nu}$$

by maximizing  $\Delta G$  to  $\Delta G_{\text{crit}}$

$$\Delta G_{\text{crit}} = \frac{16\pi\gamma^3}{3(\Delta G_v)^2} = \frac{4\pi\gamma r_c^2}{3}$$

follows

$$\Delta G_{\text{crit}} = \frac{16\pi\gamma^3\nu^2}{3(kT \ln S)^2}$$

inserted in the initial nucleation rate  $J$ , one can obtain a meaningful equation.

$$J = Ae^{\left(-\frac{16\pi\gamma^3\nu^2}{3k^3T^3(\ln S)^2}\right)}$$

This equation shows three main variables influencing the nucleation rate. These variables are the temperature  $T$ , the degree of supersaturation  $S$  and the interfacial tension  $\gamma$ .

In the **heterogeneous primary nucleation** impurities in the system act as nucleation sites. However, the same impurity in different crystallization systems can work differently and even act as an accelerator. There is no general rule and each system must be considered separately. The presence of these impurities can cause nucleation at far lower degrees of supercooling compared to the homogeneous nucleation. Therefore, the critical free energy change for the heterogeneous nucleation  $\Delta G'_{\text{crit}}$  has to be smaller than for the homogeneous  $\Delta G_{\text{crit}}$ .

$$\Delta G'_{\text{crit}} = \phi \Delta G_{\text{crit}}$$

Factor  $\phi$  is less than unity. The decrease in energy depends on the contact angle  $\theta$ , i.e. the wetting angle, of the solid phase [23]. In figure 2.4 the wetting angle is displayed. The factor  $\phi$  can be expressed as

$$\phi = \frac{(2 + \cos\theta)(1 - \cos\theta)^2}{4}$$

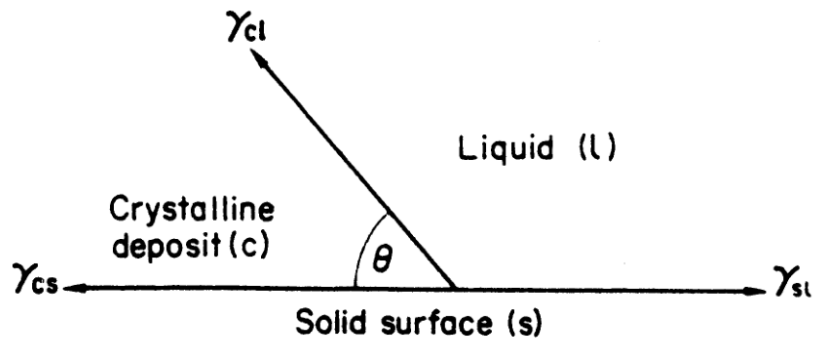


Figure 2.4: Wetting angle  $\phi$  shown by the interfacial tensions at the boundaries between two solid phases and one liquid phase [22]

### 2.2.2 Secondary nucleation

Here secondary will be used for all cases where nucleation is induced by crystals of the same type. This is caused by preexisting crystals in the supersaturated solution. New nucleation sites were formed from abrasion of these crystals by collisions between themselves, walls and internals of the crystallization device. However, there is a whole range of other mechanisms that may be responsible for the formation of new particles.

The rate of nucleation in secondary nucleation depends on the number density of crystals which are sufficiently large to undergo breakage [20]. For the nucleation rate usually a potency approach is made. It is equated with the suspension density  $M_T$ , the entered stirring power  $\epsilon$  and the supersaturation  $\Delta c$ .

$$B \propto M_T^n \cdot \epsilon^r \cdot \Delta c^l$$

whereby typically  $n=1$ ,  $r=1/2$  and  $l=1...2$  can be found.

In the industrial crystallization primary nucleation plays not a significant role, since the product particle sizes would be small and poorly controllable [20]. The design of industrial crystallization devices is therefore targeted to a complete avoidance of primary nucleation. For industrial crystallizations the driving forces for the secondary nucleation are oversaturation and input of mechanical energy. If the goal of the crystallization is to generate the greatest possible crystals, the number of nuclei must be kept low. For this purpose, the oversaturation must not be too high and the energy input into the crystallizer must be limited.

## 2.3 Crystal growth

Once in a supersaturated system nucleation sites were formed larger than the critical radius, the crystals begin to grow. Due to the complexity of the crystal growth many mechanisms have been proposed.

In the **surface energy theories**, issued by Gibbs [21], it is assumed that the shape of the growing crystal is dependent on a minimum of the surface energy. The main problems with this theory is that it was derived for spheres and the crystal growth of real crystals is not independent of their geometric shape. Furthermore, this theory also describes not the effect of supersaturation and motion of the solution on the surface of the crystals.

The **diffusion theories** assumes that mass is continuously deposited on the surface of the crystals due to concentration differences of bulk and crystal surface, similar to diffusion processes and mass transfer. Volmer [23] assumed that this accumulation is a discontinuous process that takes place in multiple layers. From this assumption the **adsorption layers theories** are followed, which have been modified in recent years.

## 2.4 MSMPR crystallizer

In this work, the concept of the so called mixed suspension mixed product removal (MSMPR) crystallizer, as shown in figure 2.5, was used to determine kinetic growth and nucleation data of VD3 and 7DHC.

### 2.4.1 Derivation utilizing population density

Randolph and Larson [25] have developed in 1988 the concept of the MSMPR crystallizer under utilizing of the population balance. This made it possible to predict the crystals size distribution (CSD) of continuous crystallizers. Several assumptions, similar to the concept of the continuous stirred tank reactor (CSTR), are involved in this formalism. First, it is assumed that no classification of the particles in the crystallizer takes place, i.e. the product CSD is the same as that found in the crystallizer. In reaction engineering this assumption would be equivalent to a defined well-mixed reaction vessel. Second, particles were assumed only to be formed by nucleation and increase in size only through growth. No secondary nucleation through breakage, attrition and other mechanisms is assumed as well as agglomeration of particles is negligible. Finally, a single characteristic size can be used to describe the entire size range as the particle shape factors are not a function of size.

By using the same approach as defining a material or energy balance, a population balance can be written for an MSMPR, figure 2.5. The number of particles entering and leaving the crystallizer in any size range  $L_1$  to  $L_2$  with population densities  $n_1$  and  $n_2$ , respectively, are

$$No.in = No.out$$

Particles can only enter or leave the size range by either growth or flow. By defining  $G$  as the growth rate of the characteristic dimension,  $V$  as the crystallizer volume and  $Q$  as the volumetric flow rate, the four terms to consider in the population balance are

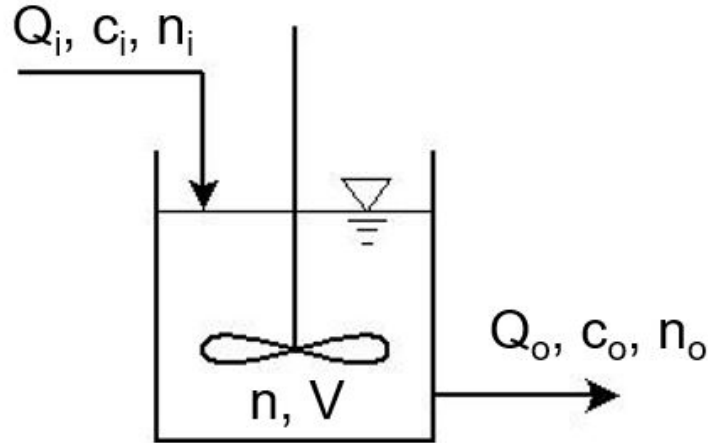


Figure 2.5: MSMPR crystallizer concept

Number of particles entering the size range by growth  $Vn_1G_1$

Number of particles leaving the size range by growth  $Vn_2G_2$

Number of particles entering the size range by flow  $Q_i\bar{n}_i\Delta L$

Number of particles leaving the size range by flow  $Q\bar{n}\Delta L$

where  $\bar{n}_i =$  average in  $L_1$  to  $L_2$  and  $\Delta L = L_2 - L_1$ . For the population balance it follows that

$$Vn_1G_1 + Q_i\bar{n}_i\Delta L = Vn_2G_2 + Q\bar{n}\Delta L$$

and with further arrangement

$$\left[ \frac{n_2G_2 - n_1G_1}{\Delta L} \right] = Q_i\bar{n}_i - Q\bar{n}$$

As  $\Delta L$  approaches zero, the mean values can be replaced by single values and result in

$$V \frac{d(Gn)}{dL} = Q_in_i - Qn$$

By defining  $\tau = V/Q$  as the mean residence times as well as assuming no particles in the feed stream, i.e.  $n_i = 0$  it results in

$$\tau \frac{d(Gn)}{dL} + n = 0$$

With consideration that the system follows McCabes  $\Delta L$  law, i.e. size independent constant growth  $G \neq G(L)$ , the equation becomes

$$\frac{dn}{dL} = -\frac{n}{G\tau}$$

This is an ordinary differential equation that can be separated and integrated. With the boundary condition at  $n(0) = n^0$  as the zero-sized particles, the final result is the well known analytical solution

$$n = n^0 \exp\left(-\frac{L}{G\tau}\right)$$

In a semi-logarithmic plot of the population density versus size, the growth rate  $G$  can be determined from the slope of the CSD as well as the zero-sized population density at the intercept.

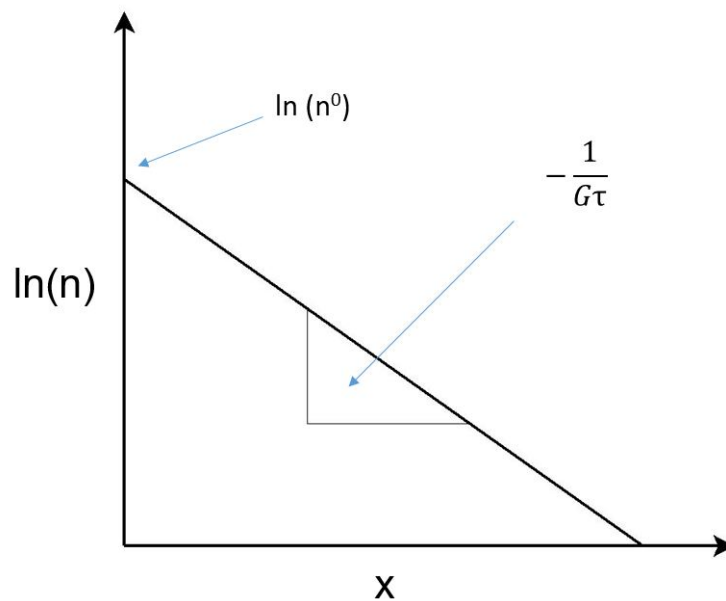


Figure 2.6: MSMPR crystallizer formalism shown in a semilogarithmic population density versus size plot [26]

The growth rate  $G$  is calculated as

$$G = \frac{1}{\text{slope}} \left(\frac{1}{\tau}\right)$$

Further, the second kinetic parameter to be obtained from the CSD is the nucleation rate  $B^0$ . It is the appearance of near zero-sized particles.

$$B^0 = \left.\frac{dN}{dt}\right|_{L \rightarrow 0} = \left[\frac{dN}{dL} \cdot \frac{dL}{dt}\right]_{L \rightarrow 0} = n^0 G$$

Plotting real data in a semi-logarithmic plot may not result in a straight line. It is possible to obtain additional information of the crystallization process from the form of the curve, according to literature [26]. Potential causes of the different types of semi-logarithmic population density plots are shown in figure 2.7. Small-size population densities often cases upward curvature of the semi-logarithmic size plot. Therefore, the data points smaller than a certain cut size were excluded in the analysis of this work.

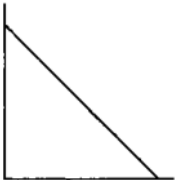

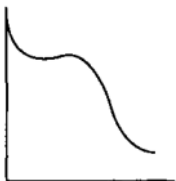
Type	Appearance	Cause
linear		MSMPR formalism is obeyed
concave upward		(i) size dependent growth rate (ii) growth rate dispersion (iii) agglomeration (iv) classification
local maxima		(i) agglomeration with breakup (ii) classification

Figure 2.7: Types of semi-logarithmic population density plots and potential causes [26]

### 2.4.2 Population density from size distribution

It is possible to translate measured crystal size distributions (CSD) into population density data with the equation [25]:

$$n = \frac{\Delta m}{k_v \rho \bar{L}^3 \Delta L}$$

Where  $\Delta m$  is the weight retained of a size fraction  $L_i$  and  $L_{i+1}$ ,  $k_v$  is the volumetric shape factor that relates the volume of a particle to its characteristic dimension cubed,  $\rho$  the particle mass density,  $\bar{L}$  the mean size of the size fraction and  $\Delta L$  the width of the size fraction. Further,  $\Delta m$  is defined as

$$\Delta m = \nu_i M_T$$

with  $\nu_i$  as the weight fraction in the size range and  $M_T$  the MSMPR suspension density.  $M_T$  can be derived from the mass balance by acknowledging equality between the time-averaged feed and product withdraw flow rates to be

$$M_T = c_0 - c$$

where  $c_0$  represents the concentration of solute in the feed and  $c$  the concentration of solute in the MSMPR mother liquor.

### 2.4.3 Growth and nucleation kinetics

With the above derived equations and by performing experiments at different process conditions, it is possible to describe growth and nucleation kinetics by commonly adopted power-law expressions of the form

$$G = k_g \Delta c^g$$

and

$$B^0 = k_b M_T^j \Delta c^b$$

where  $\Delta c = c - c^*$  with  $c^*$  as the equilibrium MSMPR concentration,  $c$  and  $M_T$  are as before. Crystals growth rate coefficient  $k_g$  and nucleation rate coefficient  $k_b$  can have Arrhenius-type temperature dependencies. However,  $k_b$  is assumed only to be a function of the hydrodynamic conditions in the MSMPR [25]. Here,  $k_g$  is expressed as

$$k_g = k_{g0} \exp\left(-\frac{E_g}{RT}\right)$$

with  $k_{g0}$  as pre-exponential factor for the growth rate,  $E_g$  as activation energy for growth,  $R$  as universal gas constant and  $T$  as temperature of the MSMPR.

In the nucleation expression,  $M_T$  is included to account the influence of supersaturation on the birth rate of new crystals. Furthermore, the influence of different stirring speeds was not accounted in this equation, but maintained constant in the experiments.

## 3 Results and Discussion

The experiments and results of this work are connected to the results obtained from VD3 batch crystallization experiments [16]. These batch experiments investigated the crystallization of vitamin D<sub>3</sub> in detail. The most important results from these experiments are:

- By assuming tBME used as solvent in the photochemical irradiation of 7DHC to VD<sub>3</sub>, a solvent switch to ACN for the crystallization of VD<sub>3</sub> after removal of tBME is a suitable method to obtain crystal yields with up to 95%.
- The amorphous state of VD<sub>3</sub> can be influenced by stirring. This finding suggests advanced micromixer concepts over normal plug-flow reactors since continuous stirring rather than single-spot mixing is needed. Due to the possibility of plugging, the concept of the MSMR appears to be the best choice.
- Linearly increasing crystallization yield with decreasing temperature.
- Temperatures below 23°C led to polymorphic form B of VD<sub>3</sub>.
- With the parameters used in the experiments either needle-shaped, columnar or prismatic crystals were obtained.
- Slightly bigger particles with a narrow PSD were obtained with a lower initial concentration and using a stepwise decrease in temperature.

The analytical instruments, equipment, evaluation methods and chemicals used in the experiments of this work are listed in chapter 6.

### 3.1 Solubility of commercial VD<sub>3</sub> in ACN

In order to develop a separation process of 7DHC and VD<sub>3</sub>, the solubility of VD<sub>3</sub> was first investigated in ACN. ACN was chosen as crystallization solvent since it shows the lowest possible solubility for both substances compared to other solvents [27]. Since tBME, the solvent used for the synthesis, has a very high solubility concerning the two substances, a solvent change to ACN in order to obtain a high yield by crystallization is necessary.

Solubility data of VD<sub>3</sub> in ACN was measured by HPLC analysis of filtrated saturated suspensions. To estimate the necessary amount of VD<sub>3</sub> at lower temperatures, the maximum solubility at 30°C was determined first. Therefore, 70 mg of VD<sub>3</sub>, an amount



slightly above the solubility at 30°C in 5 ml ACN was filled into glass vials with rolled rims. Then 5 ml ACN were added to all samples and the vials were closed with their caps. The suspensions were put into an ultrasonic bath for 10 seconds and afterwards the air in the vials was displaced by adding argon into the slightly opened cap. The vials were sealed with Parafilm® and wrapped with aluminum foil to prevent decomposition of VD3 and placed into a temperature controlled bath for approximately 24 h. After visual inspection whether still undissolved crystals were present, samples were drawn with 2 ml syringes and filtrated with 0.2 μm syringe filters into HPLC vials. The sampling and filtration was carried out as fast as possible to prevent concentration changes by dissolution or crystallization in the sample. Four samples were prepared for the temperatures 30, 20, 10, 5, 1°C. Next, the samples were analyzed via HPLC. In figure 3.1 the obtained solubility data is displayed.

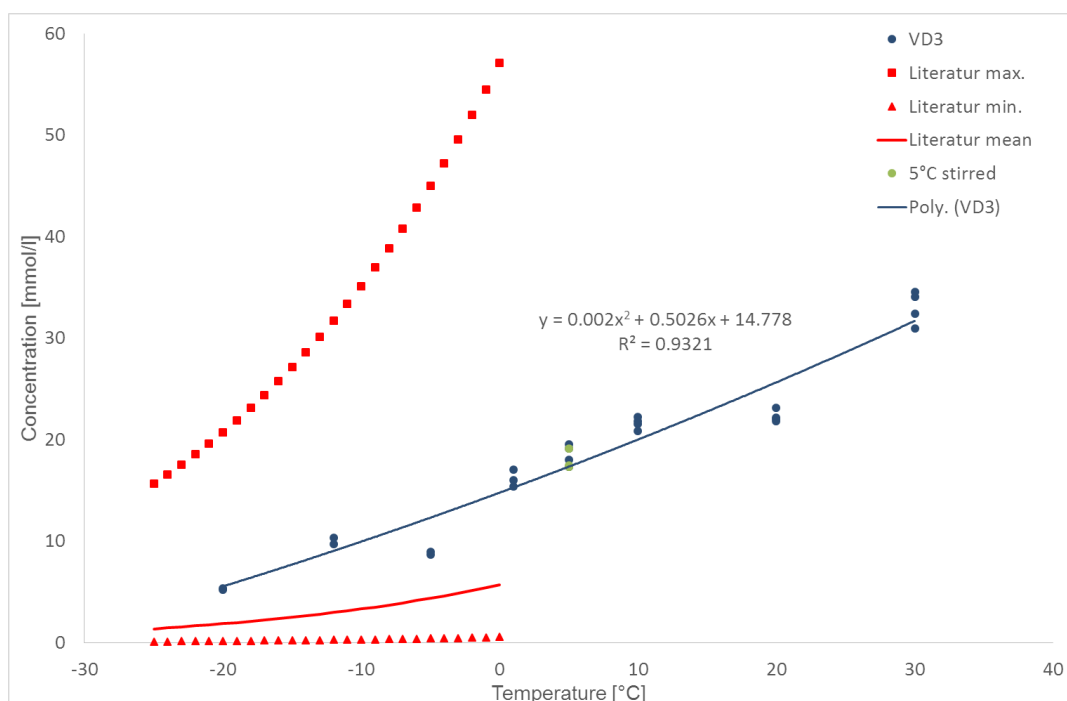


Figure 3.1: Obtained solubility data of VD3 in ACN compared to the literature [27]

Because of the long time in the temperature controlled bath a steady crystallization state was assumed. To prove this assumption, three stirred suspension at 5°C were prepared in the same way as the unstirred ones and compared to them. The samples were stirred by a cooled magnetic stirrer. For this purpose, the temperature bath of the magnetic stirrer was cooled with a brass coil in which cooling water of the thermostat was pumped through. The stirred data points are represented by the green points in figure 3.1.

The solubility curve was then extended to -20°C. Therefore the cooling liquid in the LAUDA alpha RA 12 was changed to ethanol. New points below 0°C were measured differently than before. Approximately 100 mg of VD3 were weighed into a 50 ml two-

necked round bottom flask and dispersed with 15 ml ACN. The air in the flask was displaced by argon and the flask was sealed by a KPG stirrer. Next, the mixture was short heated with a heat gun to dissolve some of the crystals. Then the flask was put into the bath, covered with aluminum foil and stirred for 5 hours. Samples were drawn with a syringe through 0.2  $\mu\text{m}$  syringe filters, put into HPLC vials and analyzed. Two samples at -20, -12 and -5°C were drawn out of the same suspension.

### Conclusion

From the course of the fitted solubility curve a crystallization of VD3 by cooling in ACN appears feasible. Furthermore, no deviation was detected in the experiments at 5°C between the stirred and unstirred samples. However, it takes more time for the non-stirred samples to reach an equilibrium state.

The obtained solubility data was compared to the literature [27] also shown in figure 3.1. A deviation from the mean value can be seen but the obtained data lies well within the limits of the literatures solubility model. The re-determination of the solubilities was also important since the solubility determination of the literature only included the temperature range of -25 to 0°C.

## 3.2 MSMPR experiments VD3

Continuous crystallization of VD3 dissolved in ACN was investigated in MSMPR experiments. Through these experiments, it should be possible to determine crystallization characteristics as described in section 2.4. Further, the feasibility of continuous crystallization of VD3 in a small laboratory setup was tested. In order to save expensive chemicals, an experimental setup was chosen which returns the discharge stream from the cooled MSMPR to the heated feed vessel. This setup can be seen in figure 3.2.

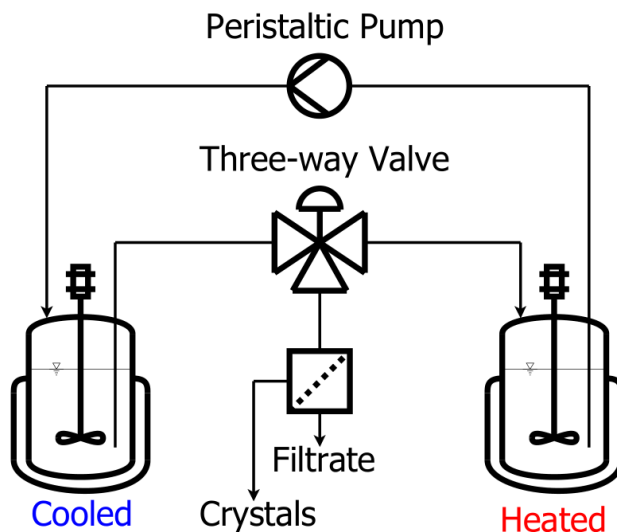


Figure 3.2: Experimental MSMPR setup for the continuous crystallization of VD3 in ACN

In this setup only one peristaltic pump was used to get rid of a regulation and level control in the MSMPR. A magnetic stirrer with temperature sensor was used for controlled heating of the feed vessel. In the experiments the MSMPR was cooled in a bath with and without applied ultrasound. As MSMPR, a 50 ml three-neck flask was used and filled until it contained 50 ml of the solution to crystallize. Afterwards, the flask was closed to be pressure-sealed. The MSMPR was stirred with a KPG stirrer, since these were tight against slight overpressure. As a connecting tube, a fluorinated ethylene propylene tube with an internal diameter of 2 mm was selected. The compounds were connected to the tubes with the BOLA joint screw system for GL 14.

Samples were drawn by switching the way of the output stream at the three-way valve. The suspension was then filtrated with a frit. Afterwards, the filtrate was analyzed via HPLC and the crystals were dried in a desiccator over night. Crystals were analyzed by microscopy, HPLC and dynamic light scattering. The input concentration of the MSMPR was measured by taking samples out of the feed vessel. During the experiment it was visually checked whether all crystals were dissolving in the feed vessel, therefore no seeding of the MSMPR was assumed. A constant filling of the MSMPR was assumed over the experiment. As a result, later drawn samples were only reducing the filling in the feed vessel. Furthermore, perfect mixing as well as no solvent loss was assumed because of the closed system. Process conditions of the experiments are shown in table 3.1.

Table 3.1: Process conditions of the MSMPR experiments with VD3 in ACN

Experiment	Flowrate	$T_{\text{Feed}}$	$T_{\text{MSMPR}}$	Ultrasound
1	5 ml/min	60°C	5°C	yes
2	5 ml/min	50°C	5°C	yes
3	5 ml/min	40°C	-10°C	no
4	5 ml/min	30°C	-10°C	no
5	5 ml/min	35°C	-8°C	yes

In Experiment 1 approximately 1.8 g VD3 were dissolved in 250 ml ACN. The same solution was used afterward in experiment 2 with an addition of 1 g VD3 to increase the concentration. Experiment 1 and 2 resulted in the formation of a sticky yellow residue stuck on surfaces of the crystallizer and tubes. This residue is referred as resin in the literature [12]. Therefore, no crystalline VD3 was obtained for the analysis.

For experiment 3, approximately 1 g VD3 were dissolved in 100 ml ACN. After the experiment, the solution was reused in experiment 4 with the addition of 4 spoons of VD3. In both experiments, the formation of the resin state could be avoided. However, a steady operation state could not be reached due to crystal agglomeration at the transition of the liquid surface to the MSMPR. At the beginning of the experiment there was turbidity in the MSMPR, which weakened after approximately 10 minutes as crystals were depositing in the MSMPR. The deposition in the MSMPR decreased the concentration in the feed vessel and after a certain time the equilibrium concentration at the temperature of the MSMPR should be reached. Therefore, no evaluation of both

experiments could be carried out.

The solution in experiment 5 consisted of 1.9011 g of VD3 dissolved in 150 ml of ACN. Since the cooling below 0°C of the ultrasonic bath was not possible with the water cooled thermostat, a cooling bath with NaCl and ice was prepared in this experiment. As a result, a temperature of -8°C could be achieved during the experiment. By introducing ultrasound, deposition in the MSMPR was prevented and the crystals remained better in suspension. However, agglomeration of the crystals remained. Due to the small tube diameter, some of the crystal agglomerates were stopping in the tube. These were made again flowable by gentle tapping. After 20 minutes, which is two times the residence time of the MSMPR, the sampling was carried out. The obtained dry crystals can be seen in figure 3.3 and the MSMPR evaluation in figure 3.4. With a selected cut size of 28  $\mu\text{m}$  and  $k_v=0.8$ , see section 2.4, the growth rate based on a characteristic dimension  $G$  was found to be 1.95  $\mu\text{m}/\text{min}$ , zero size population density  $n_0$  was  $2.54 \cdot 10^9$  [ $\#/(mm\ l)$ ] and the nucleation rate  $B_0$  was  $4.95 \cdot 10^6$  [ $\#/(1\ \text{min})$ ] for experiment 5.

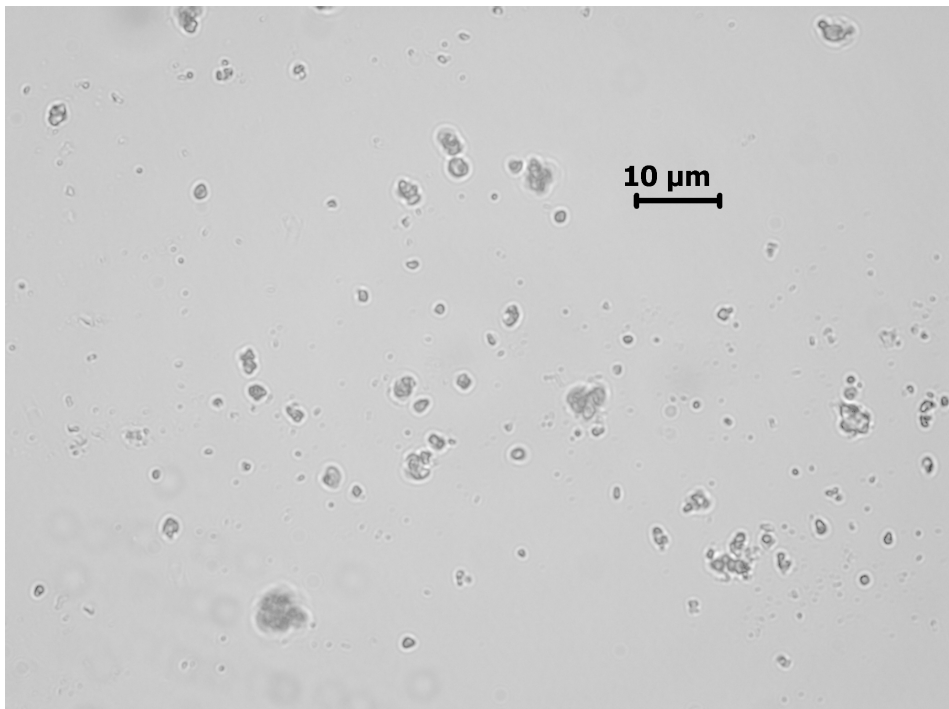


Figure 3.3: VD3 crystals prepared in MSMPR experiment 5

### Conclusion

In the MSMPR experiments, crystalline VD3 could only be produced at temperatures below -8°C. Between 5 and -8°C, there appears to be a kind of transition state in which VD3 is no longer formed in the amorphous resin form. This could probably be explained by the temperature dependency of the  $\alpha$  and  $\beta$  ratio. Furthermore, a decomposition of the vitamin during the experiment or a photochemical conversion could also contribute to the resin formation, due to the high temperatures in the feed vessel. Therefore, in the following the resin formation must be investigated in order to avoid it in later processes.

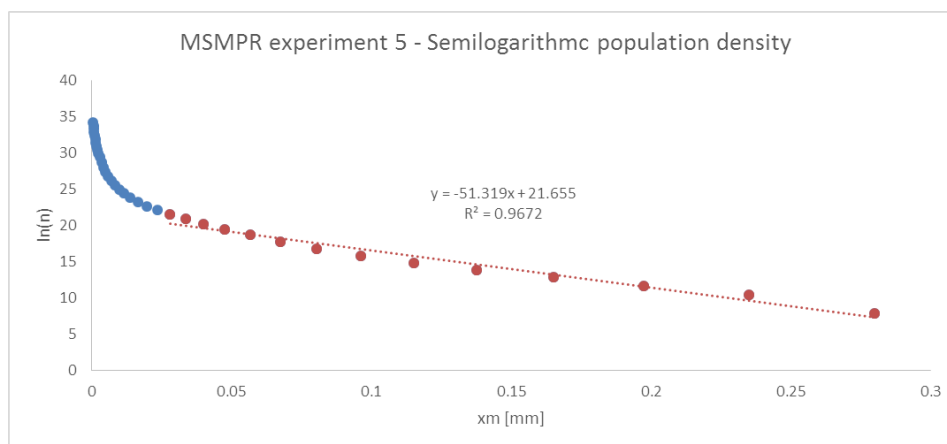


Figure 3.4: MSMPR evaluation of the population density of experiment 5 with a selected cut size of  $28 \mu\text{m}$

By recycling the MSMPR output into the feed vessel, chemicals are saved on the one hand, but no equilibrium state is reached because of deposition in the MSMPR. In order to prevent agglomeration of the crystals, the right amount of ultrasound to be inserted into the suspension must be found. Without ultrasound, the outlet of the MSMPR partly plugged due to big agglomerates and the small orifice of the tube.

### 3.3 VD3 resin

One of the main problems in the continuous MSMPR experiments was the formation of VD3-resin instead of crystallization. The produced resin stuck to tubes and moving parts and made it impossible to obtain a steady state. Therefore, a procedure to crystallize VD3 without resin formation was needed. For that approach, VD3 resin was produced on purpose and re-crystallized similar to the procedure described in [18].

Resin was made on purpose by dissolving 200.3 mg of VD3 in 1 ml tBME within a glass vial with rolled rim. The vial was then placed in a rotary evaporator at  $30^\circ\text{C}$  and 200 mbar until a honey like liquid remained. This resin was diluted with 2 ml ethyl acetate (EtOAc) and transferred into a test tube and placed in a cooling bath consisting of ice and sodium chloride. With this cooling bath it was possible to reach temperatures around  $-20^\circ\text{C}$ . Next, ACN was added as anti-solvent in  $200 \mu\text{l}$  steps to the solution. The first small crystals were observed after the addition of  $1200 \mu\text{l}$ . After  $1800 \mu\text{l}$ , turbidity was seen. Deposits on the wall were seen after  $2400 \mu\text{l}$ . After the final addition of  $3000 \mu\text{l}$ , the test tube was placed in an ultrasonic bath at room temperature. There the turbidity vanished and the remaining crystals agglomerated together into the sticky yellow resin. Back in the cooling bath, the resin lost the sticky behavior and new non-sticky white crystals were formed. The test tube was again placed in the ultrasonic bath until everything was dissolved again. Back in the cooling bath more white crystals than before were formed on the walls. To disperse the deposits on the wall, the tube

was placed for a few seconds in the ultrasonic bath and brought back into the cooling bath. Only white non sticky crystals were growing and no turbidity was observed. These crystals were transferred without filtration into a beaker, dried in a desiccator overnight. Filtration was not possible because of the low fluid amount.

81.2 mg of dried VD3 crystals were obtained and compared to the commercial VD3. This VD3 showed no difference in the HPLC analysis to the commercial VD3, i.e. no additional peaks were obtained. The obtained crystals and the commercial ones were investigated under the microscope and can be seen in figure 3.5 and 3.6, respectively.

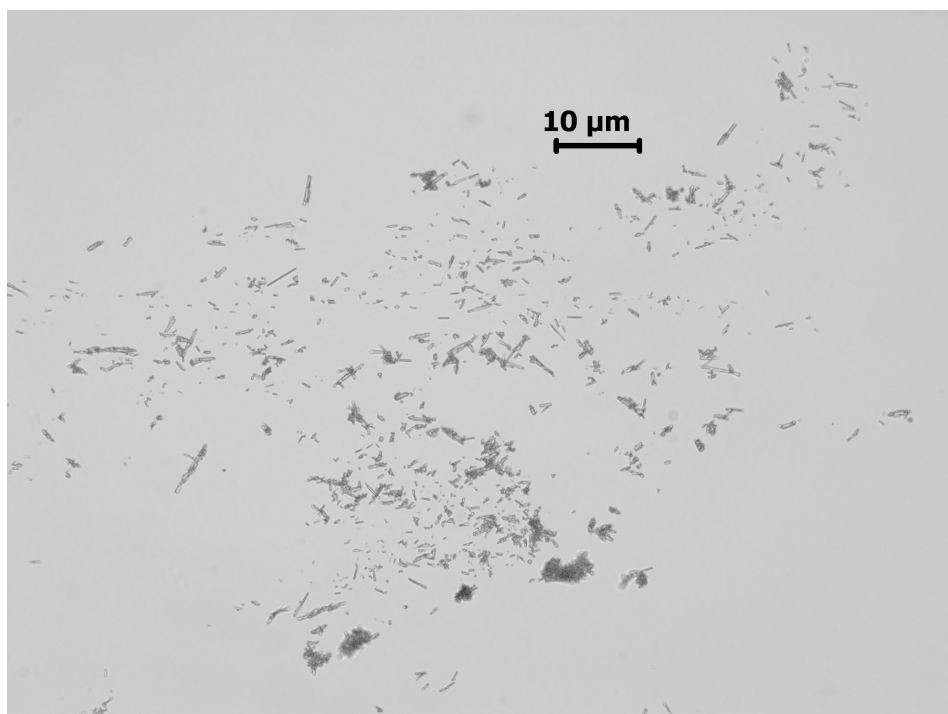


Figure 3.5: VD3 crystals obtained by re-crystallization of the commercial VD3 at  $-20^{\circ}\text{C}$  in ACN

Due to the rapid cooling, many small crystals were obtained and these were also significantly more needle-shaped than the commercial VD3. The small crystal size may also explain the white color of the resulting crystals compared to the more yellowish color of the commercial ones.

To show that EtOAc had no influence on the crystallization behavior of VD3, an experiment without it was carried out. The resin preparation was as described above. Here 201.1 mg of VD3 were used. 1 ml of ACN was added to the resin while it was stirred at room temperature. The ACN remained at the top of the resin like a drop of grease. Next, the vial was placed into the ultrasonic bath, where the resin began to form a big sticky chunk. The rest of the fluid showed a lightly white turbidity. It was not possible to obtain crystalline VD3 at room temperature. Therefore, the vial was then put into the cooling bath at approximately  $-20^{\circ}\text{C}$ . Here a strong white turbidity was seen and the resin chunk became non-sticky and brittle. Again an alternation between



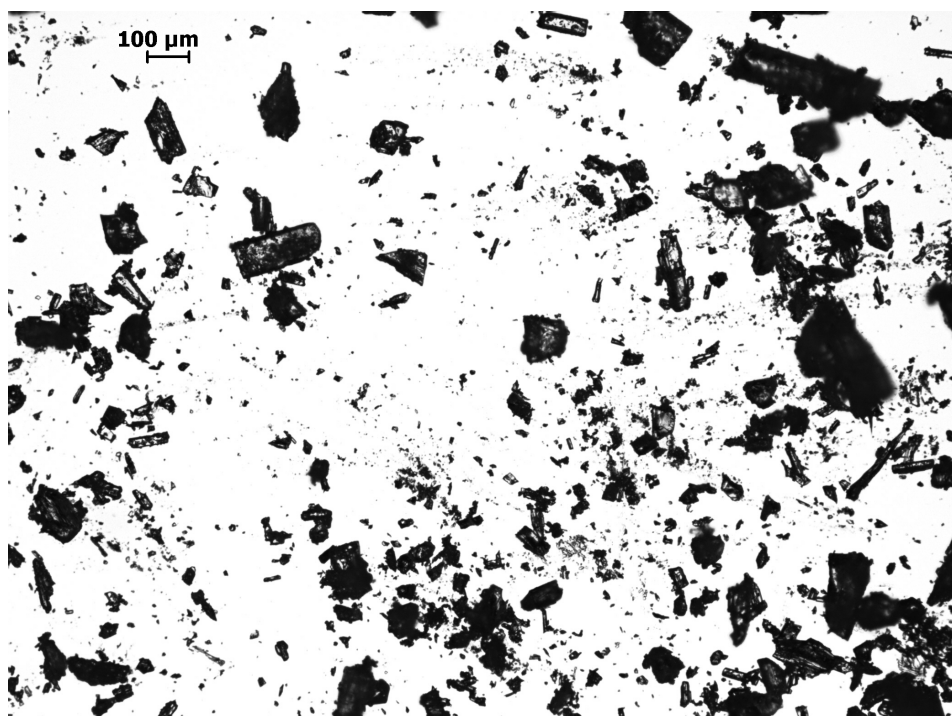


Figure 3.6: Commercial VD3 crystals directly measured

cooling and ultrasonic bath gave the non-sticky white VD3 crystals.

#### Conclusion

Anti-solvent crystallization of VD3 resin made with tBME and ACN as anti-solvent is able to produce non-sticky VD3 crystals. The addition of ethyl acetate showed no difference in the crystallization behavior of VD3. However, the low temperature at  $-20^{\circ}\text{C}$  seemed to be the key aspect in avoiding the sticky resin formation. At lower temperatures a change in crystal structure seems to occur that leads to a specific non-sticky type of VD3. The alternation between cooling and ultrasonic bath was necessary to dissolve the resin and produce nuclei from the different polymorph which was growing on the walls. No turbidity occurred after a certain amount of this new white crystals were obtained. Because of many crystallization sites, the formation of new nuclei was prevented.

### 3.4 VD3 polymorphism experiments

The experiments carried out in the previous section indicated polymorphism of VD3. In order to distinguish the respective polymorph in later experiments, Raman spectroscopy was used. The used spectrometer as well as the analytical method are listed in section 6.9. Raman spectra of VD3 produced exclusively in form B as described in section 1.1.2 should be compared to the commercial VD3.

In this work form B was prepared by dissolving 1,5 g of the commercial form A VD3 in 20 ml of tBME. Subsequently, 40ml of ACN was added and tBME as well as some of the ACN was removed at  $40^{\circ}\text{C}$  under vacuum in a rotary evaporator to achieve

supersaturation. The mass reduction by evaporation was 23.66 g. With an initial weight of 14.96 g tBME, it was assumed that the ether evaporated completely. Next, the suspension was cooled to  $-20^{\circ}\text{C}$  and alternated between the cooling and ultrasonic bath in the same way as in section 3.3. This procedure resulted again into the non-sticky crystals. After filtration with a frit, the crystals were dried in a desiccator, weighed and analyzed with Raman spectroscopy. In this experiment 0.9837 g dry VD3 in form B was produced. This corresponds to a yield of 65.6%. The spectra of commercial VD3 and the produced form B is display in figure 3.7

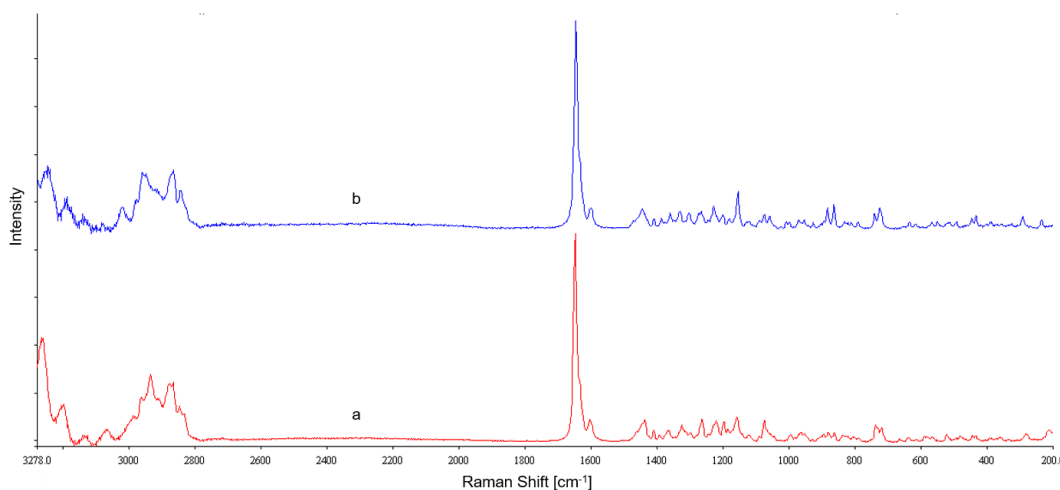


Figure 3.7: Raman spectra of VD3 **a**: commercial, **b**: form B from the experiment

### Conclusion

As described in literature [12], it was possible to produce VD3 exclusively in form B at low temperatures from a ACN solution. By using the approach in section 3.3, the alternation between ultrasonic and cooling bath to prevent the formation of the resin and favor the crystallization, it could be shown that the transition from resin to non-sticky crystalline VD3 was achieved by crystallization in crystal form B. Furthermore, it was shown that commercial VD3 is in the more stable form A.

#### 3.4.1 VD3 crystal formation and growth in ACN

Crystal formation and growth of the above introduced crystallization procedure was investigated stepwise. Seed crystals were prepared by precipitating a solution containing 101.1 mg VD3 in 5 ml ACN in a glass vials with rolled rim and cooled to  $20^{\circ}\text{C}$  in an ultrasonic bath. Before precipitation the solution was heated with a heat gun until all of the VD3 was dissolved. Next the solution was put into the ultrasonic bath at  $20^{\circ}\text{C}$  and after one minute the ultrasonic was turned on for two minutes and turbidity was seen. Samples were drawn out of the suspension, transferred on microscope slides and analyzed with a microscope. The suspension was left in the microscope slide until all of



the ACN evaporated. The image of the free-growing crystals from the microscope slide is shown in picture 3.8.

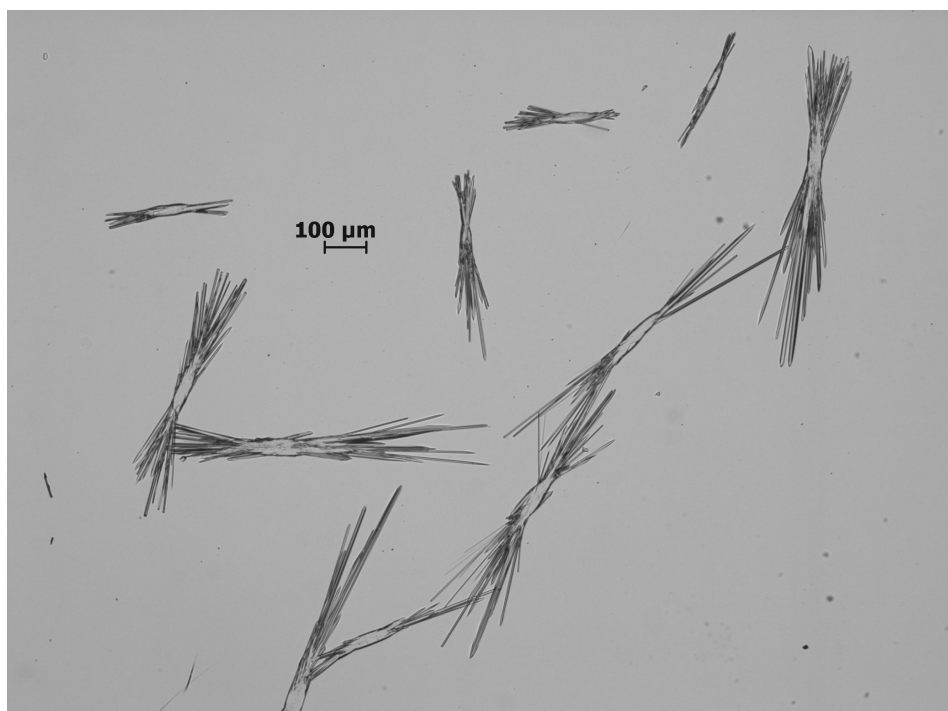


Figure 3.8: Free growing VD3 crystals on the microscope slide by slow evaporation of ACN

The seed suspension was then slowly cooled to  $-20^{\circ}\text{C}$  by briefly dipping the glass vial into the cooling bath. Despite the presence of many seeds and slowly

cooling, crystals were growing on the glass walls. The vial was then alternated between the ultrasonic and cooling bath to produce crystals as described in the previous section. Agglomeration of the produced crystals was seen and the turbidity vanished. A sample was drawn out of the suspension with a pipette, transferred on a microscope slide and directly analyzed with the microscope, see picture 3.9. The remaining crystals were dried in a desiccator and analyzed via Raman spectroscopy. Crystal form of the produced crystals was compared to the commercial VD3.

### Conclusion

As described in section 2.2.1, nearly all of the small nuclei were dissolved in favor of the growing larger crystals. This was seen in case for the free growing crystals on the microscope slide and after the formation of crystal agglomerates. Despite plenty nuclei formation after the ultrasonic treatment, the crystal growth induced by the temperature difference was too fast and crystals grew on the surface of the vial. The freely growing crystals showed a dendrid like form, whereby the crystal agglomerates being needle-shaped. A Raman evaluation of the free-growth crystals was not possible due to the small amount. However, due to the different crystal shape and by the fact that the crystals formed at  $-20^{\circ}\text{C}$  showed again form B, it was assumed the crystals on the slide

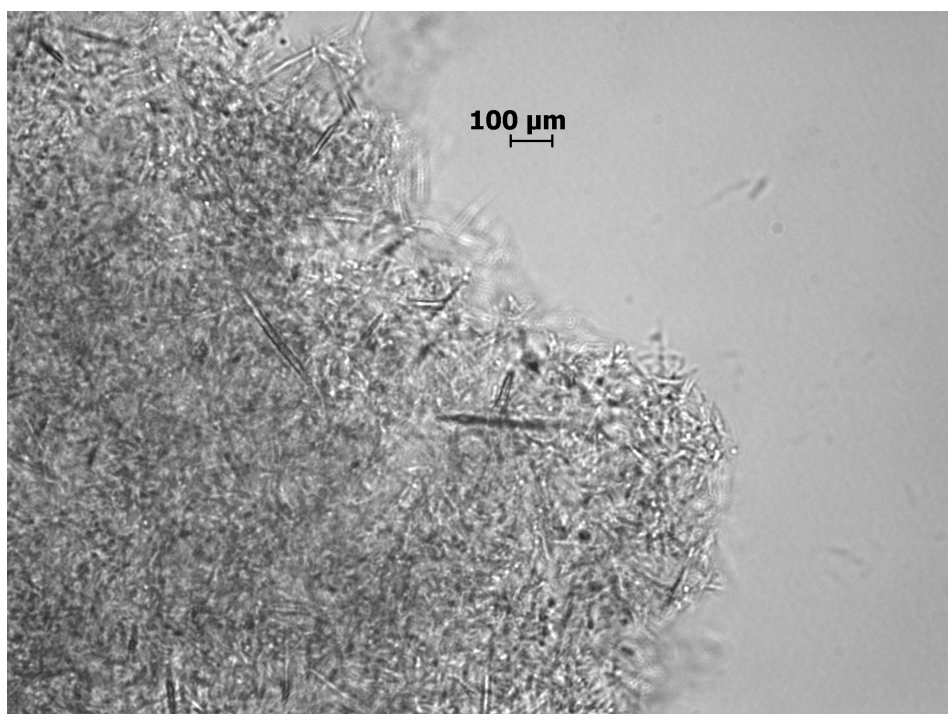


Figure 3.9: Agglomerated VD3 crystals in suspension obtained by re-crystallization of commercial VD3 at  $-20^{\circ}\text{C}$

were form A.

Another point in which polymorphs can be different is their solubility. Therefore, the solubility of VD3 form B should be determined and compared with the solubility data of the commercial VD3 in form A obtained in section 3.1.

### 3.4.2 Solubility of VD3 form B in ACN

Since polymorphs can have different solubilities, the solubility of the specifically prepared VD3 in the form B from section 3.4 was determined as described in section 3.1. The obtained solubility is displayed in figure 3.10. In order to prove that the obtained solubility belongs to the respective crystal form, the polymorphic form of the remaining crystals was determined with Raman spectroscopy. At  $-20$ ,  $-10$  and  $10^{\circ}\text{C}$  the crystal form remained B. It was not possible to obtain enough crystals at  $25^{\circ}\text{C}$  for the analysis due to resin formation. Therefore, this temperature point and for comparison, the temperature point at  $10^{\circ}\text{C}$  was again examined.

#### Conclusion

After the determination of the solubility, the evaluation of the remaining dry crystals with Raman spectroscopy showed new peaks at a Raman shift of approximately  $2850$  and  $1780\text{ cm}^{-1}$  in all samples, figure 3.11. However, it could be shown that crystal form B was preserved in all experiments.

Furthermore, there was some kind of reaction between  $10$  and  $25^{\circ}\text{C}$  which lead to

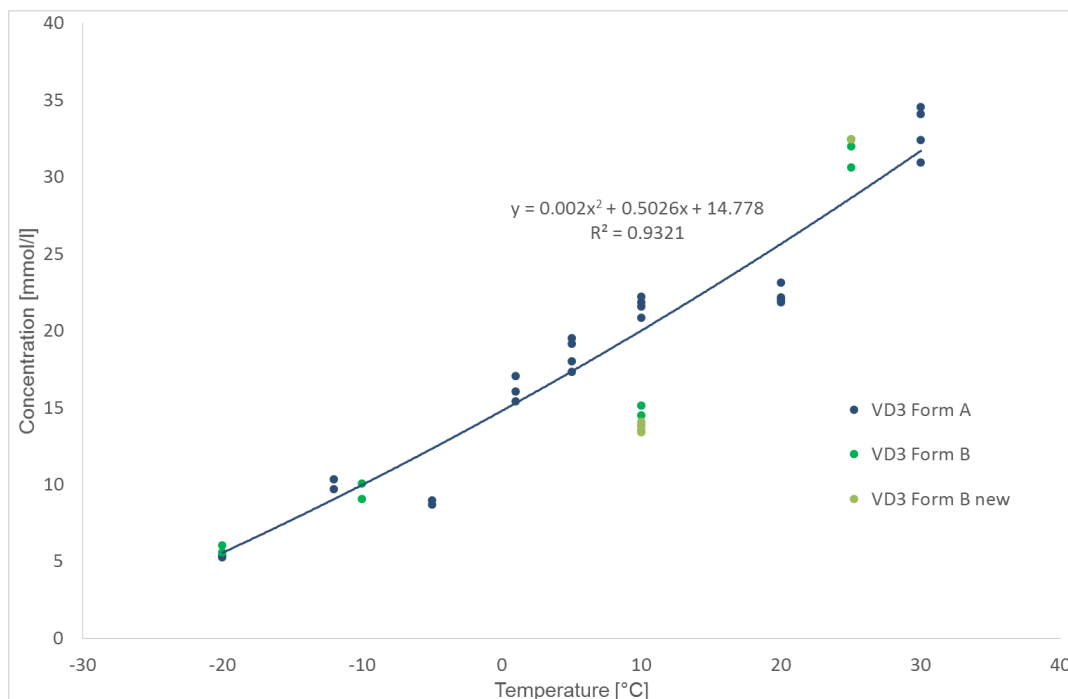


Figure 3.10: Solubility of the different polymorphic forms of VD3 in ACN

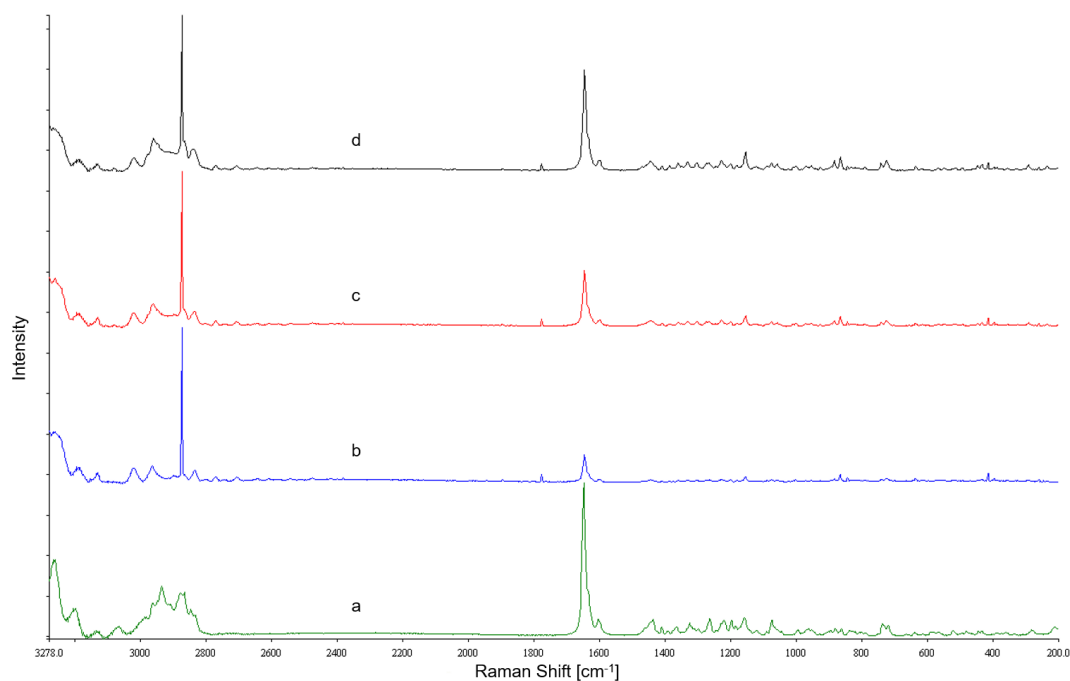


Figure 3.11: Raman spectra: **a** commercial VD3, **b** sample crystallized at 10°C, **c** sample crystallized at -10°C, **d** sample crystallized at -20°C

agglomeration and sticky behavior of crystals. The samples at -20 and -10°C remained in a well dispersed suspension. This change was also detected in the HPLC evaluation of the samples. The difference occurred between the samples at 10 and 25°C in the beginning of the chromatogram. The comparison of the two temperature points after 300 min at 210 nm can be seen in figure 3.12.

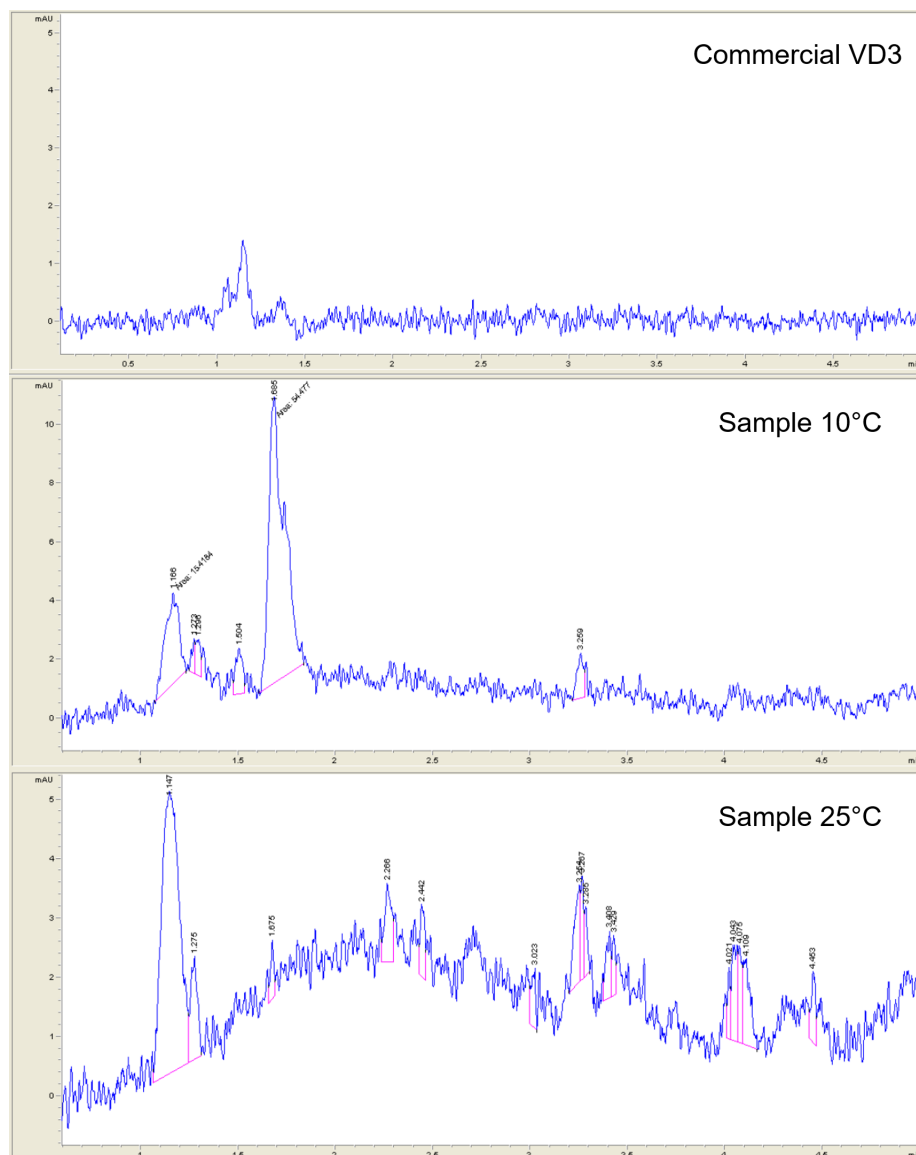


Figure 3.12: Zoom of the front part of the HPLC chromatogram of commercial VD3 and VD3 directly measured after 300 minutes at 10 and 25°C in ACN to show possible reactions

Decomposition by oxygen and photochemical reactions of the vitamin in the vials was excluded, since the samples were darkened, stored under argon and sealed. The most plausible possibility is the reverse reaction of form B to the pre-vitamin, which

consists only of the unstable alpha conformer. This reverse reaction is favored at higher temperatures. During the reverse reaction, some alpha conformers might break down, which would also explain the new peaks in HPLC and Raman. The reaction of the alpha conformer could also be one of the reasons for the formation of the VD3 resin.

Since the obtained solubility points did not deviate very much from the obtained curve of the form A, the solubility curve of form A will be used further in this work for the design of the separation process.

### 3.5 Solubility 7DHC in ACN

To obtain an overview of the possible separation of 7DHC and VD3 via crystallization, the solubility of 7DHC in ACN was determined and plotted with the data obtained for VD3.

The solubility curve of 7DHC was studied by adding an amount of 7DHC well above the solubility limit into a 50 ml round bottom flask and dispersing it with 15 ml ACN, put directly in the temperature bath of the thermostat and stirred with a KPG stirrer for 5 hours. The weighted amounts of 7DHC for the investigated temperature points at -20, -10, 15, 25 and 30°C were 30.4, 51.1, 80.0, 60.3 and 102.2 mg, respectively. Samples were covered with aluminum foil during the experiment, to prevent photochemical reactions. Then two samples were drawn out of the same suspension and filtrated through a 0.2  $\mu\text{m}$  syringe filter into HPLC vials. The filtrate was analyzed via HPLC and the obtained data was added to the solubility data of VD3 in figure 3.13.

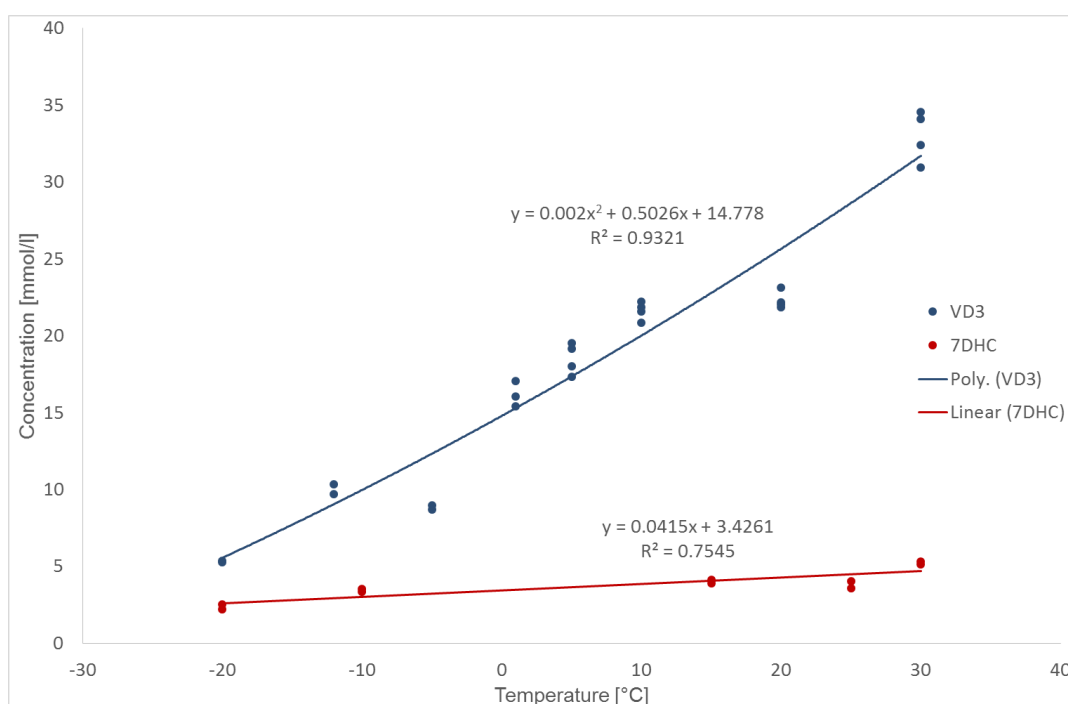


Figure 3.13: Solubility data of VD3 and 7DHC in ACN

### Conclusion

Since the fit of the obtained data points with a polynomial approach represented almost no difference to a fit with a straight line, for simplicity reasons the solubility curve of 7DHC was approximated by a straight line.

The advantage of cooling crystallization can be recognized by the low solubility and slope of the 7DHC solubility line compared to VD3. With a cooling crystallization starting from right to left in the solubility diagram, comparatively much more VD3 than 7DHC would crystallize.

## 3.6 MSMPR experiments with 7DHC

7DHC is the second important chemical substance of this work, since it is still present in large quantities after the synthesis it has to be separated. Therefore the crystallization characteristics of 7DHC in ACN were determined.

In the same way as in section 3.2, MSMPR experiments were carried out. The same experimental setup was used. The process conditions are shown in table 3.2. The MSMPR was directly mounted in the cooling bath. Two experiments were carried out with 3 operating points (OP) each and without the application of ultrasound. Samples were drawn after 15 minutes after the temperature in the MSMPR remained constant at the set flow rate. For experiment 1, 1.201 g 7DHC were dissolved in 150 ml ACN. After experiment 1, the remaining solution and suspension was mixed, stored cooled overnight and then re-used in experiment 2.

Table 3.2: MSMPR experiments with 7DHC in ACN

	Experiment 1			Experiment 2		
	OP1	OP2	OP3	OP1	OP2	OP3
$T_{\text{Feed}} [^{\circ}\text{C}]$	60	60	60	60	60	60
$T_{\text{MSMPR}} [^{\circ}\text{C}]$	-20	-15	-10	-20	-15	-10
$F_{\text{in}} [\text{ml}/\text{min}]$	10	10	10	7.5	7.5	7.5
$\tau [\text{min}]$	5	5	5	6.7	6.7	6.7
$c_{\text{In}} [\text{g}/\text{l}]$	5.729	5.160	3.327	4.094	2.621	2.133
$c_{\text{Out}} [\text{g}/\text{l}]$	2.023	1.610	1.736	1.751	1.454	1.398
$c^* [\text{g}/\text{l}]$	0.999	1.078	1.158	0.999	1.078	1.158
$M_{\text{T}} [\text{g}/\text{l}]$	3.71	3.55	1.59	2.34	1.17	0.73
$G [\text{mm}/\text{min}]$	0.00390	0.00458	0.00378	0.00427	0.00316	0.00337
$n^0 [\#/(mm\ l)]$	$7.58 \cdot 10^9$	$2.42 \cdot 10^9$	$2.88 \cdot 10^9$	$1.68 \cdot 10^9$	$2.13 \cdot 10^9$	$1.21 \cdot 10^9$
$B^0 [\#/(l\ \text{min})]$	$2.95 \cdot 10^7$	$1.11 \cdot 10^7$	$1.09 \cdot 10^7$	$7.19 \cdot 10^6$	$6.73 \cdot 10^6$	$4.10 \cdot 10^6$

The obtained growth rate over the supersaturation is shown in figure 3.14. The figure shows at the operating points at  $-20^{\circ}\text{C}$ , that the growth rate at lower supersaturation is higher than at higher temperatures. However, this is not possible and may be caused by the formation of deposits in the MSMPR. Therefore, these operating points were skipped in the further evaluation.

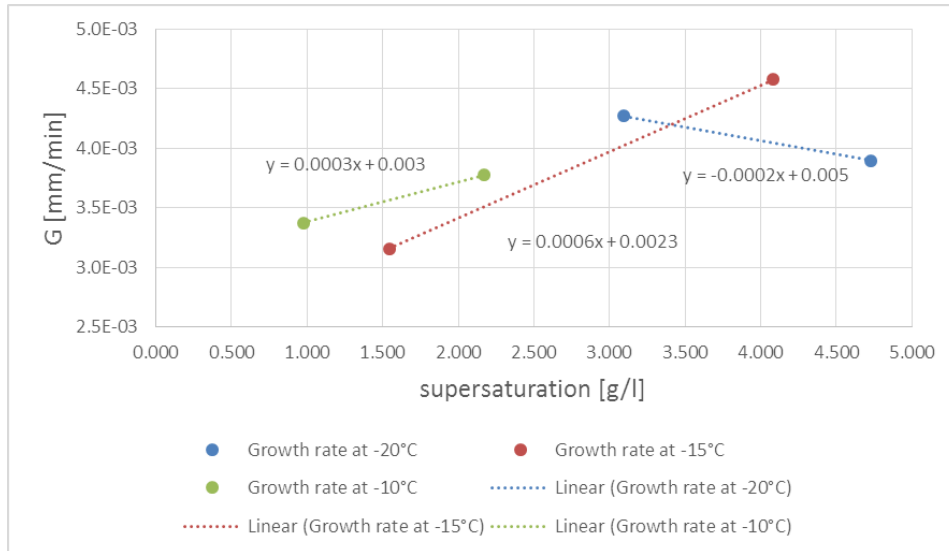


Figure 3.14: Crystal growth rate over supersaturation

Growth rate equation from section 2.4.3 was linearized, fitted in figure 3.15 and the temperature points  $-10$  and  $-15^\circ\text{C}$  were evaluated. This gave a pre-exponential factor for the crystal growth rate  $k_{g0}$  with  $5.356 \times 10^{-21}$  [(mm/min)/(g/l)] and an activation energy for growth  $E_g$  with  $-90.065 \text{ kJ/mol}$ .

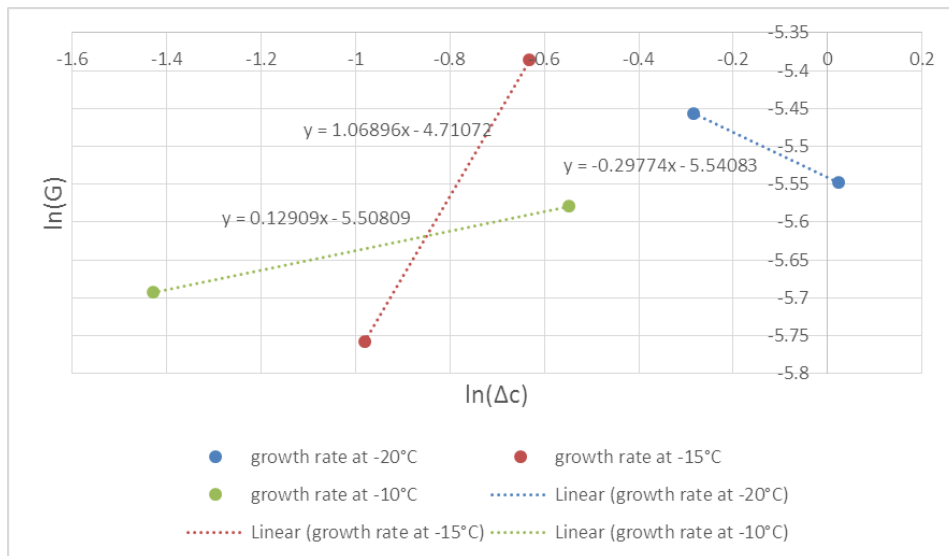


Figure 3.15: Fit crystals growth rate

### Conclusion

In the MSMRP experiments with 7DHC, the same problems as with the VD3 MSMRP experiments occurred again. Due to the deposition in the MSMRP, an equilibrium state was prevented. The constant accumulation of 7DHC in the MSMRP can also be seen by



an decreasing input concentration of the feed. Therefore, the data concerning growth, might not be very accurate and can only be used as rough guidance.

Especially in experiment 2, there was some formation of sticky residue in the MSMPR. This formation could have been caused by reactions of the 7DHC, because of the high feed vessel temperature.

An experiment with a flow rate of 5 ml/min was also carried out. However, at this flow rate crystals were deposited after the MSMPR in the tube. At even lower flow rates a pulsating flow or slug flow should be used to prevent settling of crystals.

### 3.7 Separation Process

To achieve the goal of this work, i.e., the separation of VD3 from 7DHC directly after the synthesis, the obtained solubilities are used to develop a separation process by cooling crystallization. Starting point of the following experiments is a mixture which corresponds to a conversion of 30% after the irradiation part of the industrial process, section 1.2, at the maximum solubility of 0.22 mol/l or 0.084 g/ml VD3 in tBME at 25°C. Since both substances have very high solubilities in tBME, a solvent switch to ACN has been planned to favor crystallization. Cooling and anti-solvent batch experiments, as well as a continuous experiment in an MSMPR were carried out.

#### 3.7.1 Batch experiments

To design a separation coupled directly after the synthesis, batch experiments were performed. These batch separation experiments are divided into two separation steps, with 7DHC planed to be separated in the first step and VD3 being obtained in the second step. The starting solution to crystallize consisted of 7DHC and VD3 in tBME with concentrations comparable to solutions out of the reactor with 30% conversion. The used amounts of chemicals are shown in table 3.3.

Table 3.3: Batch experiments with two separation steps

No.	Sample weight			Separation 1						Separation 2					Filtrate	
	7DHC [mg]	VD3 [mg]	tBME [ml]	Temp. [°C]	ACN [ml]	Time [min]	Crystals dry			Temp. [°C]	Time [min]	Crystals dry			Content 7DHC [%]	Content VD3 [%]
							Amount [mg]	Content 7DHC [%]	Content VD3 [%]			Amount [mg]	Content 7DHC [%]	Content VD3 [%]		
1	61.7	25.9	1	25	2.5	40	46.4	95.70	4.30	-20	60	18.7	44.88	55.12	2.50	97.50
2	59.9	26.4	1	25	15	40	40.7	97.76	2.24	-20	60	10.6	47.85	52.15	6.78	93.22
3	59.1	25.5	1	25	2.5	90	61.7	85.11	14.89	-10	60	4.9	58.90	41.10	2.30	97.70
4	149.2	67	2.5	25	5	17	41.9	85.68	14.32	-20	90	15.6	47.42	52.58	4.01	95.99
5	26.8	166.6	0	25	15	120	27	0.00	100.00	-20	120	85.3	21.46	78.54	7.19	92.81
6	59.7	28.9	0	25	30	120	0	not enough crystals	not enough crystals	-20	120	32.3	93.99	6.01	41.48	58.52
7	148.7	64.5	2.5	25	15	20	102.4	98.58	1.42	-20	20	1.6	30.01	69.99	12.76	87.24



The procedure of experiments one to three is displayed in figure 3.16. The solutions were transferred into Schlenk-tubes and stirred at 25°C under reduced pressure at 300 mbar. After 5 minutes the pressure was set to 250 mbar and the solution began to boil. The solvent was evaporated until no visible boiling could be seen and a high viscous fluid remained. Then ACN was added in different amounts as displayed in table 3.3. Crystals were formed immediately after addition of this anti-solvent. Ultrasound was applied to enhance the mixing and remove the crystals on the walls. Ultrasound was applied to enhance the mixing and remove the crystals on the walls.

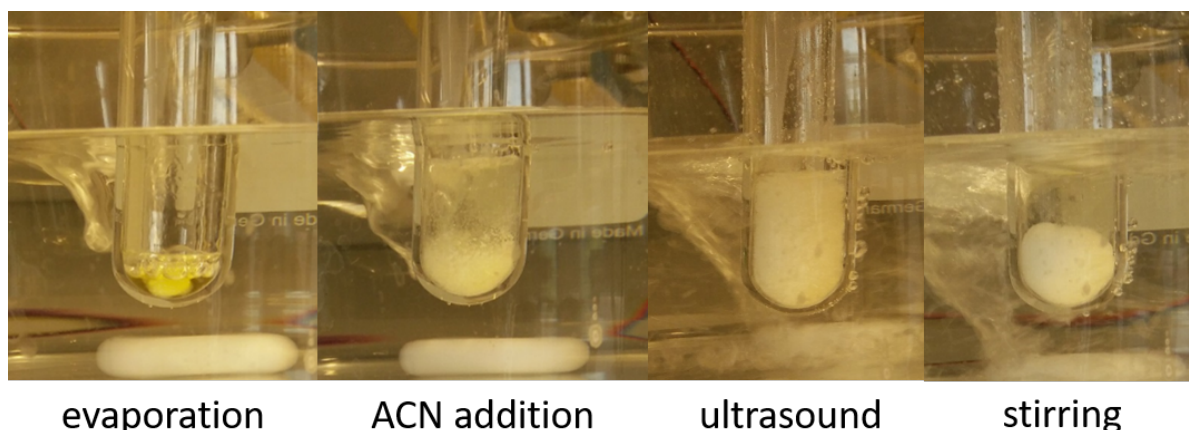


Figure 3.16: Batch steps for experiment one to three

Experiments four and seven were carried out by evaporation of the ether from a mixture including ACN and tBME. This was done in stirred Schlenk-tubes at 40°C under a reduced pressure starting from 300 mbar to 120 mbar in 30 minutes. The used quantities are given in table 3.3. In experiment four, 3.743 g solvent were evaporated. With a starting value of 1.875 g tBME and 3.960 g ACN it was assumed that all of the ether evaporated. To increase the flow ability of the suspension, 5 ml ACN were added. Experiment seven included 1.869 g tBME and 11.909 g ACN. Here, 8.770 g solvent were evaporated.

In experiments five and six no ether was used and the suspensions were made directly in ACN. These experiments should serve as a comparison to assess the influence of the ether on the evaporation and crystallization. Furthermore, an excess of VD3 was used in experiment five.

After the respective batch time at 25°C, see table 3.3, the suspensions were filtrated with a frit and the crystals were dried in a desiccator. A sample for HPLC analysis was drawn out of the filtrate. Next, the filtrate was alternated before separation 2 between a cooling bath without stirring and an ultrasonic bath to produce the non-sticky crystals as described in section 3.3. Thereafter, the suspensions were placed in the cooling bath without stirring at the temperature and times given in table 3.3.

The samples were filtered after the displayed times and the filtrate was analyzed again by HPLC. Crystals were dried in the desiccator and the produced crystal amounts and corresponding batch conditions can be seen in table 3.3. Content in the table represents in context of crystals the composition of the solid crystal mixture and in the context

of filtrate the composition of the solution by assuming only the two substances present. As an example of the relation of filtrate content and concentration, the concentration of experiment four is shown in figure 3.17.

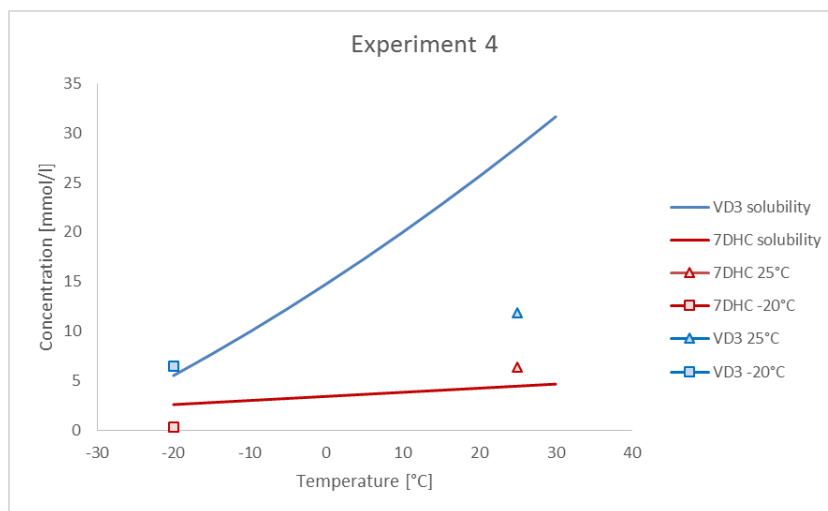


Figure 3.17: Concentrations in the filtrate of experiment 4 after separation 1 and 2 at 25 and -20°C, respectively

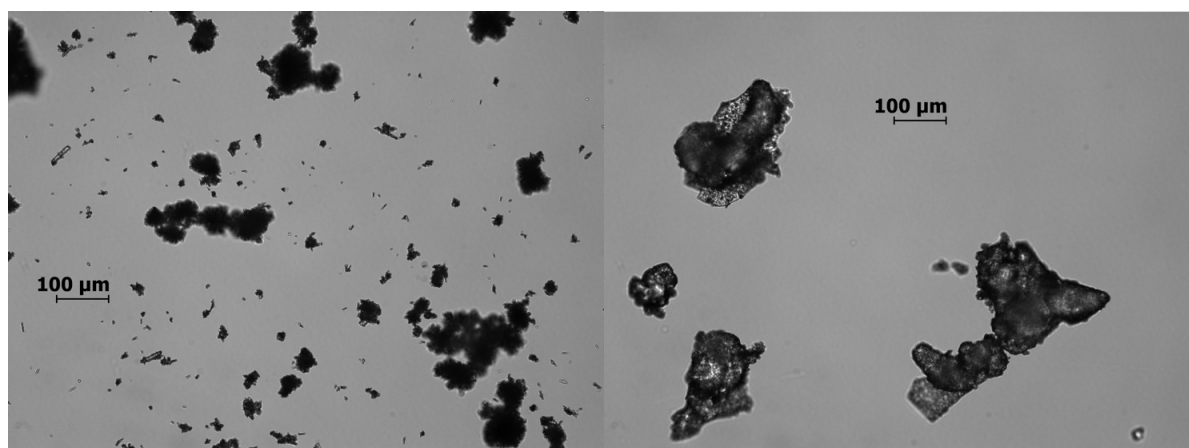
### Conclusion

In the experiment with tBME the obtained crystals by filtration after separation 2 were melting together in the desiccator. This can be seen in figure 3.18 by the obtained crystals of experiment one. Since these crystals were mainly consisting of VD3, a VD3 resin formation could have occurred. Despite this, the starting solvent mixture does not influence the product ration, however the evaporation of tBME first is much faster. Furthermore, crystals after the first separation were forming agglomerates as well as some larger needle-shaped crystals as seen in figure 3.18 on the left hand side.

By comparing experiment one and three, a time dependency affecting the crystallization yield in separation 1 was seen. At longer crystallization times, a greater yield was obtained. Also in Experiment 7, a lower crystal yield in separation step 2 was achieved by a short crystallization time.

From the experiments something very interesting was observed in the second separation step. A far lower concentration of 7DHC was measured in the filtrate than the solubility curve would predict, see figure 3.17. This could be caused by a co-crystallization of 7DHC together with VD3 as described by Mei [28]. Through this effect a higher separation than it can be concluded from the solubility data can be achieved. It was possible to separate more than 98% of 7DHC from the starting solution.

Since there is still a great amount of VD3 and almost no 7DHC in the filtrate after the separation step 2, it should be recovered. This could be done by evaporation of some solvent and again crystallization at low temperatures or by an anti-solvent crystallization. For reasons of simpler process design, the anti-solvent crystallization will be investigated in more detail.



Experiment 1: dry crystals after separation 1

Experiment 1: dry melted crystals after separation 2

Figure 3.18: Obtained crystals of experiment 1

### 3.7.2 Antisolvent batch experiments

In the first experiment the anti-solvent crystallization with water added to a mixture of VD3 and E321 dissolved in ACN will be tested. Water was chosen since it is cheap, non-toxic and VD3 is completely insoluble in it. Here E321 will be used as an internal crystallization standard to calculate with dilutions. E321 was chosen because it is also used as an antioxidant in the industrial process [5].

First a solution containing 51.4 mg VD3 and 19.4 mg E321 dissolved in 5 ml ACN, or more precisely 3.9565 g ACN, was prepared. This solution was heated to 30°C with a magnetic stirrer. Stepwise 200 µl water was added. A strong turbidity was seen after the addition of 1 ml water. At 1600 µl, bigger crystals were formed on the walls. After the addition of 2 ml, the turbidity vanished and only crystals were remaining in the suspension. The suspension was then brought into the ultrasonic bath for a short time and then placed again in the bath at 30°C. Another 1 ml water was added to the stirred suspension and after 15 minutes the sample was filtrated with a frit. After filtration the crystals were washed with ACN at -20°C and dried in the desiccator. 31.3 mg of dry crystals were obtained and analyzed with HPLC. No trace of E321 was found in the HPLC evaluation. Therefore, E321 was used as an internal standard in the next experiment.

Within the second experiment, the anti-solvent crystallization with water after separation 1 described in section 3.7.1 will be investigated. A solution was prepared corresponding to the filtrate after step 1. It consisted of 148.1 mg 7DHC, 64,2 mg VD3 and 25,9 mg E321 dissolved and filled up with ACN in a 15 ml volumetric flask. This solution was mixed with different amounts of water and stirred at 25°C for 60 minutes. The experiments were carried out in 10 ml vials with rolled rims, closed with their caps and stirred with magnetic stir bars. In diagram 3.19 the concentration in the remaining filtrate of these batches is shown. For the sake of clarity, samples 1 and 2 are additionally shown in the solubility diagram at 25°C on the left hand side of the diagram.

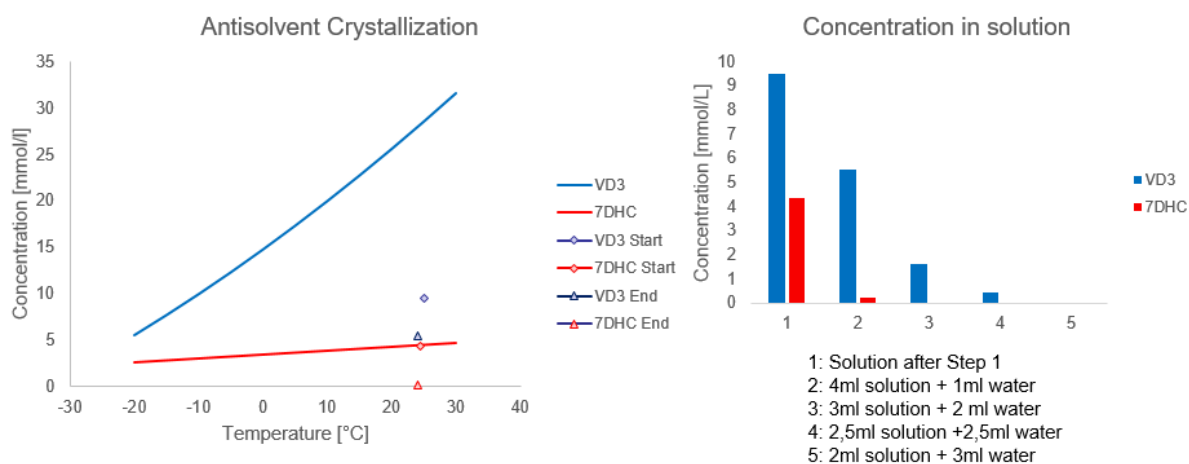


Figure 3.19: Separation of VD3 and 7DHC in ACN with water as anti-solvent at 25°C

### Conclusion

From these experiments it can be concluded that anti-solvent crystallization is a good alternative to cooling crystallization. It is possible to achieve the same results as by cooling crystallization compared to the second separation step. Even the effect of co-crystallization seems to occur. Therefore, it was also possible to separate nearly all of the 7DHC from the solution.

Furthermore, no of the E321 was found in the HPLC analysis by dissolving the remaining crystals of the suspension in tBME. Therefore, E321 can be used as internal standard for the anti-solvent crystallization. Directly after addition of water, there was turbidity formed with subsequent agglomeration. However, in all experiments with anti-solvent, resin was later formed on the magnetic stir bars after approximately 15 minutes.

### 3.7.3 Antisolvent MSMPR experiment

In this experiment the separation of the VD3 in the filtrate obtained after the second separation described in section 3.7.1 was tested in continuous mode in an MSMPR with anti-solvent crystallization. The experimental setup can be seen in figure 3.20. The anti-solvent, water, was added directly before the MSMPR. Therefore, no seeding was assumed and an evaluation of the experiment according to chapter 2.4 was carried out. The concentration reduction caused by the dilution was analyzed with E321 as internal standard. As shown in the anti-solvent batch experiments in section 3.7.2, E321 remains in solution after addition of the anti-solvent and is therefore suitable as an internal standard.

Before the start of the experiment, the crystallizer was filled. This was done by pumping into the open flask with the feed and anti-solvent pump at 3 and 2 ml/min, respectively for 10 minutes. The feed solution consisted of 212.1 mg VD3 and 79.7 mg E321 dissolved in 100 ml ACN. The crystallizer was then sealed tightly and after 5 minutes the experiment was started with the same pump rates as when filling. Throughout

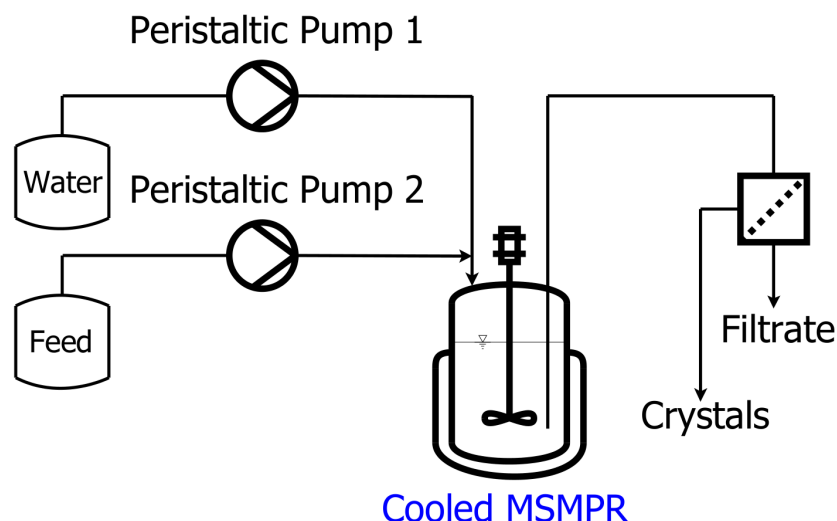


Figure 3.20: MSMPR anti-solvent setup for the continuous crystallization of VD3

the 15 minutes experiment, the temperature of the cooled ultrasonic bath was at 23.8°C. All of the output crystals were collected with a frit and dried in a desiccator. In- and output concentrations were analyzed from the feed solution and the accumulated filtrate, respectively.

Particle size distribution of the obtained crystals was measured as described in section 6.8. The obtained distribution is displayed in figure 3.21. After this measurement the suspension was examined under the microscope, picture 3.22. Furthermore, the crystals were dissolved in tBME and analyzed by HPLC. Finally, the crystal form was determined by Raman spectroscopy shown in figure 3.23.

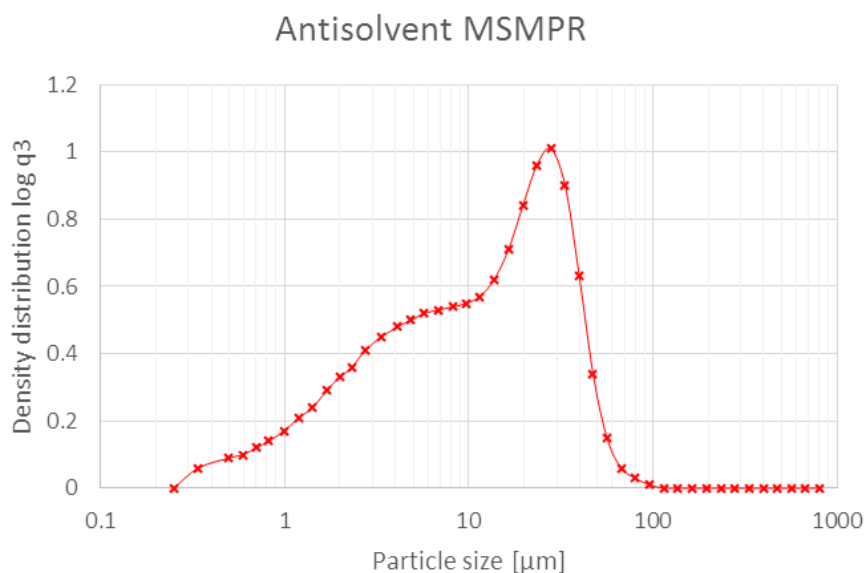


Figure 3.21: Density distribution of the product of step 3



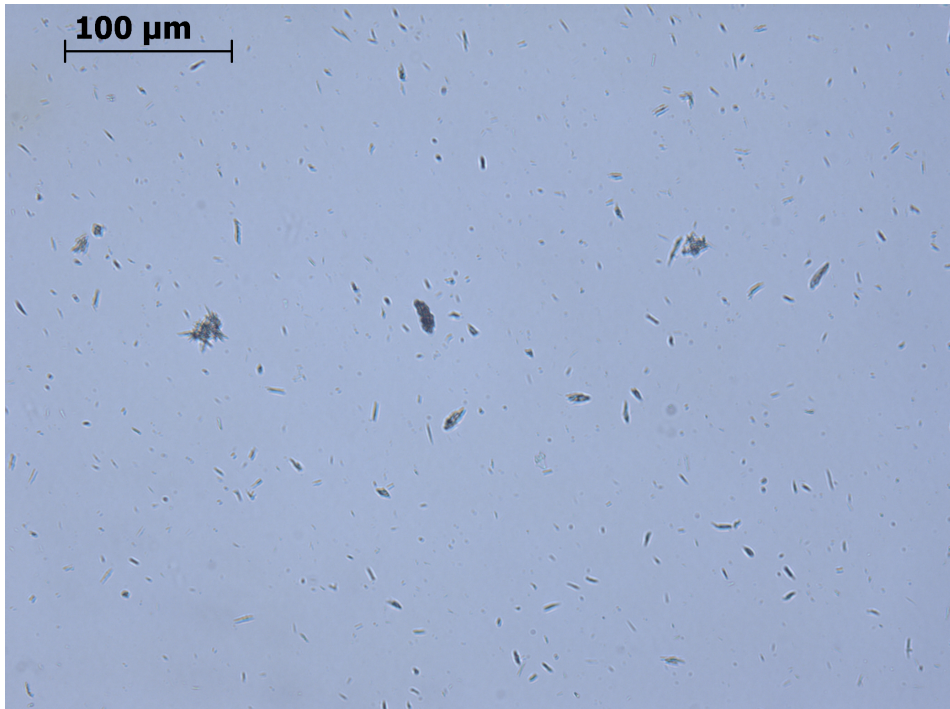


Figure 3.22: VD3 product crystals of step 3 suspended with a surfactant in water

Through the evaluation of the experiment the diagram 3.24 was produced. As  $k_v$ , 0.8 was chosen because of the small and short needles. Particle density  $M_T$ , as described in section 2.4.2, was  $0.969 \text{ g/cm}^3$  and the residence time was 10 minutes. With a selected cut size of  $6.25 \text{ μm}$ , the growth rate based on a characteristic dimension  $G$  was found to be  $0.616 \text{ μm/min}$ , zero size population density  $2.5 \cdot 10^{11} \text{ [#/(mm l)]}$  and the nucleation rate  $1.54 \cdot 10^8 \text{ [#/(1 min)]}$ .

### Conclusion

By avoiding higher temperatures, the equilibrium conversion of VD3 could be avoided and crystals of the more stable form A were produced as indicated at the significant regions in the Raman evaluation displayed in figure 3.23. Furthermore, the resin formation was avoided at this conditions but the small crystals were agglomerating. This agglomeration can be seen by the high peak in the density distribution in figure 3.21 as well as in the microscope pictures in figure 3.22. Due to the short experiment time compared to the residence time, the obtained crystallization data can only be used as a rough guide, since a equilibrium state of process may not be reached.

At this point, it should be mentioned that the same experiment was carried out in a tubular crystallizer with a length of 3.8 m, at the same process conditions and with the same crystallization solution. In this experiment it was not possible to filter crystals, since they were too small and were not retained by the frit. Due to the shorter residence time of approximately 2.4 minutes, the growth time for the crystals could have been too short. Furthermore, no agglomeration of the crystals was detected in this experiment, wherein during the filling process of the MSMPR agglomeration occurred after approximately 6 minutes. As a result, a certain time is needed for the crystal

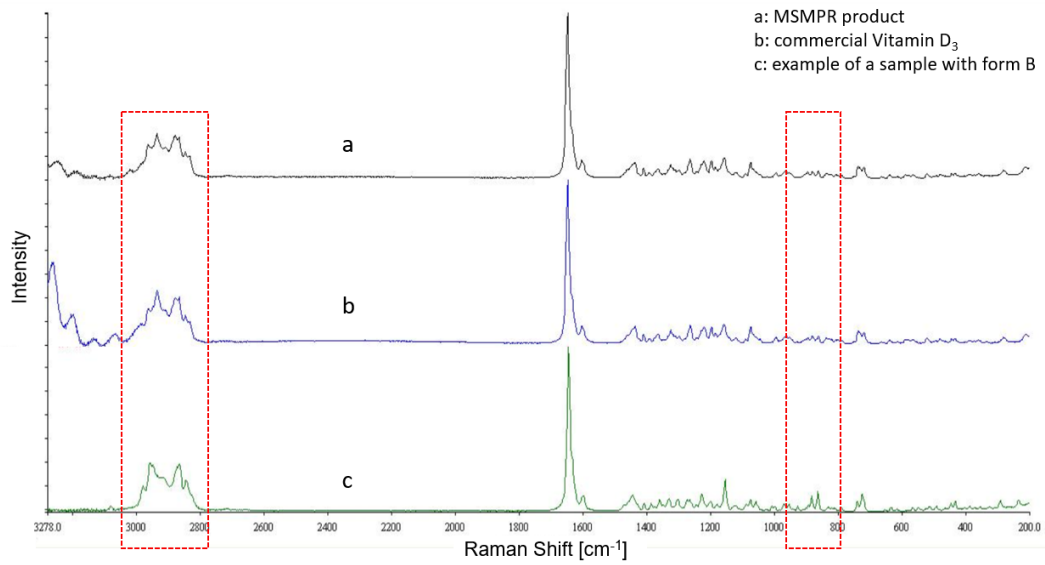


Figure 3.23: Raman spectra of step 3 product

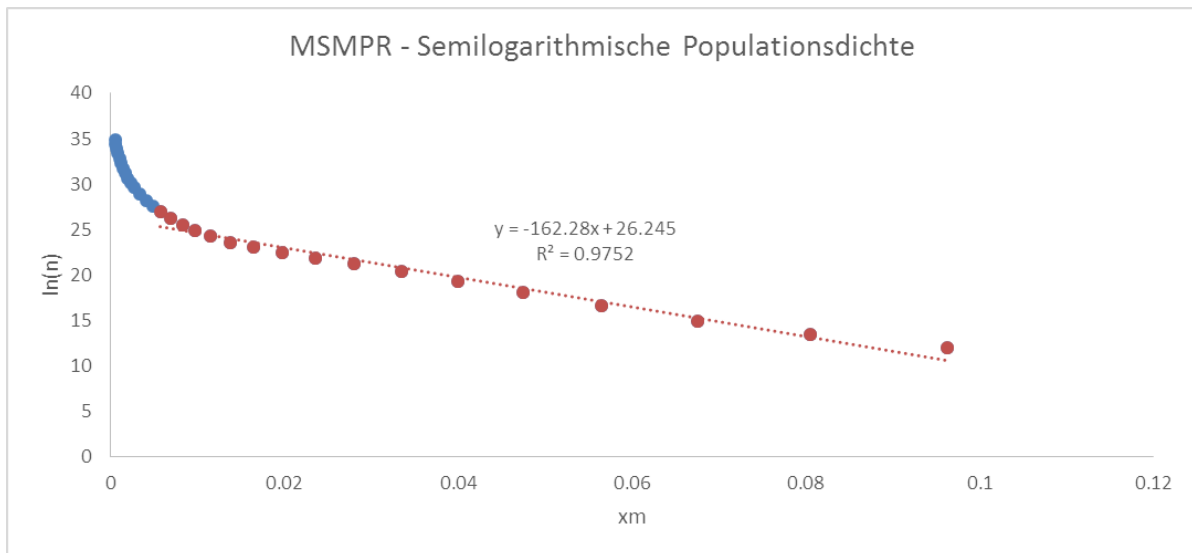


Figure 3.24: MSMPR evaluation of the semilogarithmic population density of step 3 with a selected cut size of 6.25  $\mu\text{m}$

growth to achieve crystals large enough to agglomerate. Future experiments dealing with the kinetics of crystallization should provide these necessary data.

### 3.7.4 Proposed separation process

From the obtained experimental data, a three step separation process through crystallization was developed. This process is shown in Figure 3.25.

In Step 1, a solvent switch from tBME to ACN takes place to separate most of the 7DHC. This solvent switch is necessary since crystallization directly from a tBME solution is difficult to achieve due to the high solubility of 7DHC and VD3. However, the temperature during the solvent switch should not be selected too high to avoid unintended reactions. Whereby, the ACN quantity should be chosen slightly above the solubility curve of VD3 obtained in section 3.1 at a temperature of approximately 30°C to prevent any loss of vitamin. Step one is particularly important because the synthesis had only a conversion of 20-30% and a large amount of 7DHC has to be separated. The crystals obtained from the first separation step contain almost exclusively 7DHC and can be re-used for the synthesis.

Next, step 2 is a purification step to remove almost the entire 7DHC. The effect of co-crystallization of 7DHC and VD3 as described in section 3.7.1 is used. Either anti-solvent or cooling crystallization could be possible. A cooling crystallization at low temperatures of at least -10°C is proposed. For the anti-solvent crystallization, however, lower temperatures should also be used to prevent the resin formation of the vitamin. The crystal mixture of this step could be recycled back into step one.

Finally step 3 is the crystallization step of VD3. Here a temperature controlled anti-solvent separation can be carried out to control polymorphism. In the experiment in section 3.7.3, an anti-solvent crystallization with water at room temperature was carried out. The addition of anti-solvent directly before the MSMR caused the formation of many nuclei. A certain residence time is necessary for this process step in order to form larger crystal agglomerates. However, if VD3 resin formation occurs, the crystallization could be carried out at lower temperatures at around -10°C. At this temperature the resin state would be avoided and the resulting VD3 would then probably be in the crystal form B.



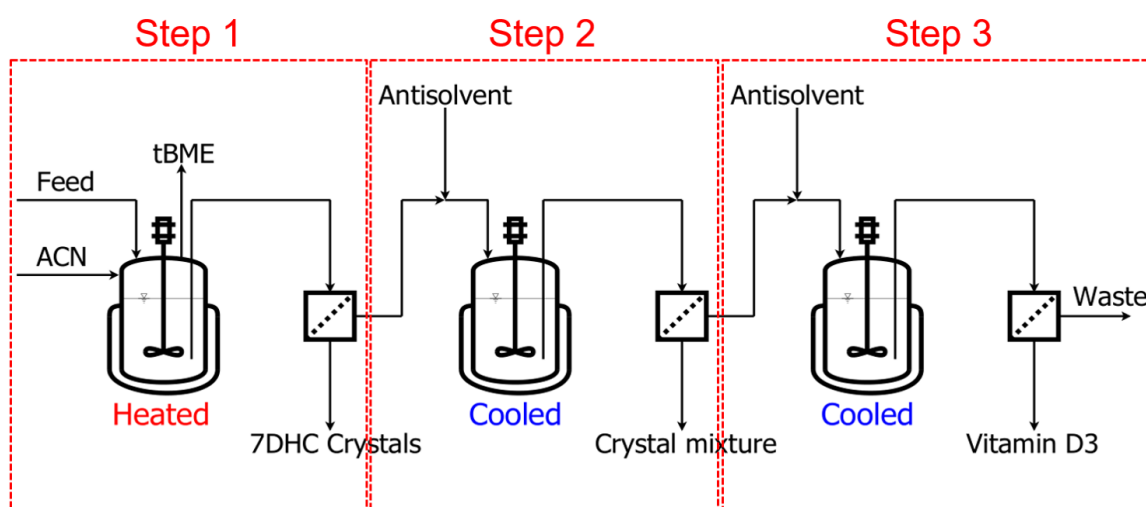


Figure 3.25: Proposed 3 step process to separate VD3 and 7DHC. Step 1: Solvent switch to ACN because of the high solubility of the used ether to separate most of the 7DHC. Step 2: Further purification were almost all of the 7DHC is separated. Either anti-solvent or cooling crystallization could be possible. Step 3: Temperature controlled anti-solvent crystallization of VD3 to control polymorphism

## 4 Summary

- **Solubility**

Solubility data of commercial VD3 and 7DHC in ACN were obtained in batch experiments. From the course of the fitted solubility curve, cooling crystallization in ACN appears feasible. A comparison to literature data [27] showed a deviation, however, the obtained data in the corresponding region was well within the limits of the literature's solubility model.

- **MSMPR experiments**

MSMPR experiments were carried out with VD3 and 7DHC to obtain crystallization data. In the experiments with VD3, there was a formation of a sticky residue in the MSMPR which is referred as resin in the literature[12]. This resin prevented a steady operation state of the MSMPR by depositing in the MSMPR and tubing. Crystalline VD3 was only obtained at temperature below  $-8^{\circ}\text{C}$ . However, there was still deposition in the MSMPR. From the 7DHC experiment, crystallization data was obtained, but a steady state was again not reached due to deposition of the crystals in the MSMPR. A possibility to prevent crystallization on the glass surface of the MSMPR would be to use ultrasound or faster stirring to create more nuclei. Furthermore, problems by sedimentation of crystals at low flow rate were seen. Pulsating flow or slug flow should be used to prevent settling of crystals.

- **Polymorphism**

The prevention of the resin formation was then investigated because of the problems caused in the MSMPR experiments. Similar to the procedure described in [18], VD3 resin was produced on purpose and tried to re-crystallize. To produce the resin, VD3 was in this work dissolved in tBME and then the ether was evaporated until a honey like liquid remained. ACN was then added as anti-solvent and the suspension was alternated between an ultrasonic bath at room temperature and a cooling bath at  $-20^{\circ}\text{C}$ . With this procedure it was possible to produce non-sticky VD3 crystals. The low temperature seemed to be the key aspect in avoiding the sticky resin formation, whereby the alternation between cooling and ultrasonic bath was necessary to dissolve the remaining resin and produce nuclei of the non-sticky crystals. This non-sticky VD3 crystal form was later identified as the polymorph form B. This polymorph only consists of the  $\alpha$  conformer of the vitamin as described in [12]. The used commercial VD3 was identified as form A. In solution, VD3 exists as a dynamically equilibration mixture of  $\alpha$  and  $\beta$  conformers. Their ratio was reported to be temperature and solvent dependent [13, 14, 15]. As

described in literature [12], it was possible to produce VD3 exclusively in form B at  $-20^{\circ}\text{C}$  from a ACN solution.

Solubility of the obtained VD3 form B in ACN was then investigated and compared to the commercial VD3. A reaction of the dissolved form B vitamin at temperatures above  $10^{\circ}\text{C}$  seemed to take place. This was seen by agglomeration of crystals as well as in the Raman and HPLC evaluation. Since the obtained solubility points did not deviate very much from the obtained curve of the form A, only the solubility curve of form A was used in the other experiments of this work.

- **Batch separation**

Based on the obtained solubility data, batch experiments were carried out to investigate the separation of VD3 and 7DHC by cooling crystallization. Starting point of the experiments was a mixture which corresponds to a conversion of 30% after the irradiation part of the industrial process [5] at the maximum solubility of 0.22 mol/l or 0.084 g/ml VD3 in tBME at  $25^{\circ}\text{C}$ . In two separation steps, more than 98% of the 7DHC was removed from the solution. This high separation was possible through co-crystallization with the vitamin and led to concentrations far below the solubility of 7DHC in ACN. The remaining filtrate after the second separation step consists for the most part of VD3 and is subsequently crystallized.

Anti-solvent crystallization with water after the above mentioned separation step 1 was investigated. A solution was prepared corresponding to the filtrate after step 1 and water was added with different amounts. It was possible to achieve the same results as by cooling crystallization compared to the second separation step. Even the effect of co-crystallization seemed to occur. Furthermore, E321 was found to be a suitable internal crystallization standard to calculate with dilutions.

- **Anti-solvent MSMPR**

The separation of the VD3 dissolved in the filtrate obtained after the two separation steps was investigated in continuous mode in an MSMPR with anti-solvent crystallization. Directly before the MSMPR, the anti-solvent water was added to the feed. This resulted in the formation of many nuclei and can be seen by a high nucleation rate of  $1.54 \cdot 10^8$  [ $\#/(1 \text{ min})$ ]. The concentration reduction caused by the dilution was compensated with the aid of E321 as internal standard. By avoiding higher temperatures, the equilibrium conversion of VD3 to more  $\alpha$  conformers could be avoided and crystals of the more stable form A were produced.

- **Proposed separation process**

On the basis of the obtained experiments, it was possible to propose a separation process for 7DHC and VD3. The process consists of three steps. In Step 1 a solvent switch to ACN takes place and most of the 7DHC can be separated and re-used in the synthesis. Step 1 is particularly important because the synthesis might have only a conversion of 20-30% and a large amount of 7DHC has to be separated.

Next, Step 2 is a purification step where almost all of the 7DHC is separated. Either anti-solvent or cooling crystallization could be possible. The Crystal mixture of this step could be recycled back into step 1. Finally step 3 is the crystallization step of VD3. Here a temperature controlled anti-solvent crystallization can be carried out to control polymorphism.

## 5 Outlook

In future work, the proposed separation process for 7DHC and VD3 should be optimized. Furthermore, all separation steps should be tested in continuous mode directly coupled to each other. Here influences of impurities from the synthesis may affect the separation. One of the most challenging tasks might be the continuous filtration between the process steps.

Formation of the different VD3 polymorphs has to be studied in detail to prevent the resin formation. Especially between the temperature range of 10 to 25°C in ACN. Also, the influence of different anti-solvents on the polymorphism should be tested since water as anti-solvent resulted in the more desired form A of the vitamin. Furthermore, the influence of ultrasound on the formation of different polymorphs should be investigated.

Continuous crystallization in an MSMR promised good results. However, the stirring power of the MSMR used in the experiments was low. With higher energy input either by ultrasound or better stirring, the agglomeration in the crystallizer should be prevented. Therefore, further attempts to determine crystallization kinetics should be carried out.

Possible co-crystallization of 7DHC and VD3 in separation step 2 which resulted in 7DHC concentrations far below its solubility in ACN should be studied. This effect occurred by cooling and anti-solvent crystallization.

## 6 Methods and Materials

### 6.1 High pressure liquid chromatography - HPLC

HPLC analysis was carried out with an Agilent 1100 series HPLC system (Agilent, Waldbronn, Germany), equipped with an online degasser, quaternary pump, autosampler, thermostatted column compartment and UV-visible diode array detector. A reversed phase column  $50 \times 4.6 \text{ mm}; 2.7 \mu\text{m}$  Agilent Poroshell 120 EC-C18 was used as stationary phase.

In the HPLC method, acetonitrile was used as mobile phase. The flow rate was set to 0.5 ml/min with a run time of 15 minutes at a column temperature of 25°C. A sample injection volume of 0.1  $\mu\text{L}$  into the HPLC system was set. UV-detection was performed at 210, 260, 280 and 300 nm. The samples taken were directly measured without further pretreatment.

#### 6.1.1 HPLC calibration

Calibration of VD3 and 7DHC was carried out by preparing solutions in 2 ml of tBME displayed in table 6.1 and 6.2, respectively. The corresponding diagrams are shown in figure 6.1 for VD3 and figure 6.2. For the evaluation of the experiments mainly signal trace D at 300 nm was used. Retention times of VD3 and 7DHC were 8.0 and 10.2 minutes, respectively.

Table 6.1: Calibration VD3

$C_{\text{target}}$ [M]	VD3 [g]	tBME [g]	$C_{\text{calibr.}}$ [mM]	A 210nm	B 280nm	C 260nm	D 300nm
0.2	0.1557	1.4762	189.0	41184.7	38730.4	47716.9	9471.8
0.15	0.1163	1.4832	143.0	32605.2	30392.1	37379.4	7223.6
0.1	0.0777	1.4849	97.1	22183.1	20433.2	25526.2	4885.3
0.05	0.0390	1.4899	49.5	10203.1	9478.8	11836.9	2270.8
0.01875	0.0143	1.4853	18.4	4268.2	3914.2	4936.4	946.2

In the experiments, E321 was added with a maximum of 1% weight of the total solution. The highest concentration for calibration was calculated with 3% weight of 2 ml ACN. Solutions were prepared in 2 ml ACN and are shown in table 6.3. The obtained calibration can be seen in figure 6.3. Evaluation of experiments was done with signal trace B at 280nm. The retention time of E321 was 1.68 minutes with this method.

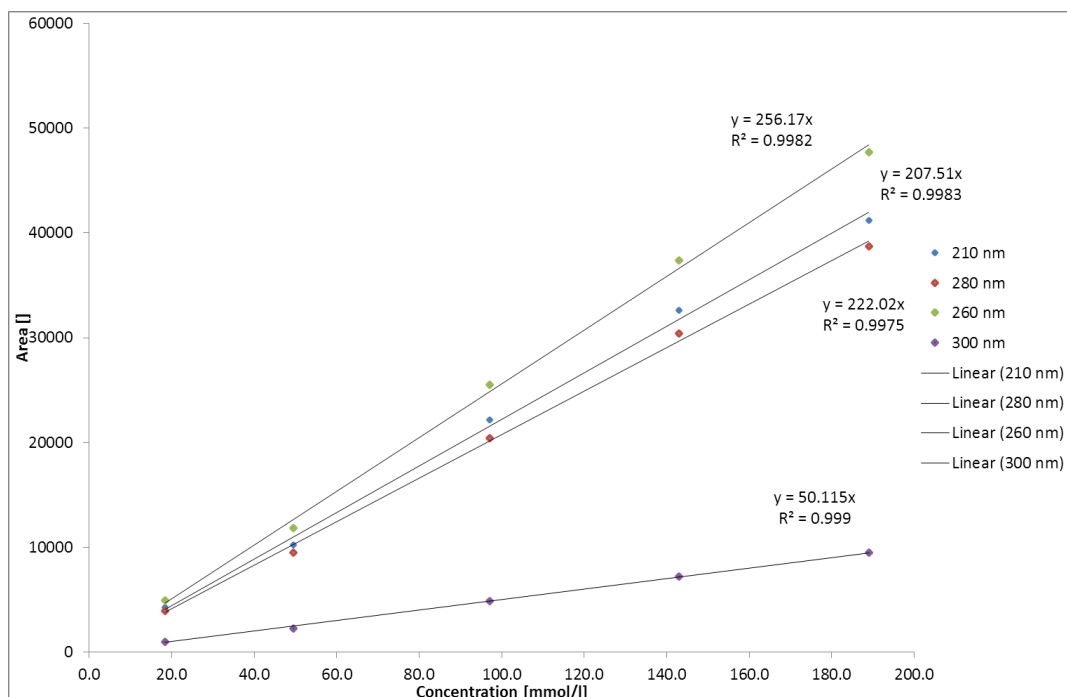


Figure 6.1: HPLC calibration of VD3. Area versus concentration

Table 6.2: Calibration 7DHC

$C_{\text{target}}$ [M]	7DHC [g]	tBME [g]	$C_{\text{calibr.}}$ [mM]	A 210nm	B 280nm	C 260nm	D 300nm
0.2	0.1557	1.4744	189.2	4756.2	19108.0	11657.5	5464.9
0.15	0.1185	1.4812	145.8	3892.3	15717.1	9583.4	4514.1
0.1	0.0757	1.4765	95.2	2529.9	10422.4	6323.0	3018.4
0.05	0.0394	1.4810	50.3	1321.0	5402.5	3286.3	1546.0
0.01875	0.0144	1.4739	18.7	482.7	1995.0	1192.3	575.7

Table 6.3: Calibration E321

$C_{\text{target}}$ [M]	E321 [g]	ACN [g]	$C_{\text{calibr.}}$ [mM]	A 210nm	B 280nm	C 260nm	D 300nm
0.1063	0.0653	1.5938	141.4	15365.7	3727.4	1012.1	25.4
0.0709	0.0334	1.5948	73.2	9060.9	1673.7	455.1	11.0
0.0532	0.0230	1.5912	50.7	6634.6	1162.1	318.9	8.8
0.0354	0.0156	1.5966	34.4	4773.6	809.9	219.9	5.9
0.0177	0.0090	1.5938	19.9	3150.3	520.4	140.9	4.1

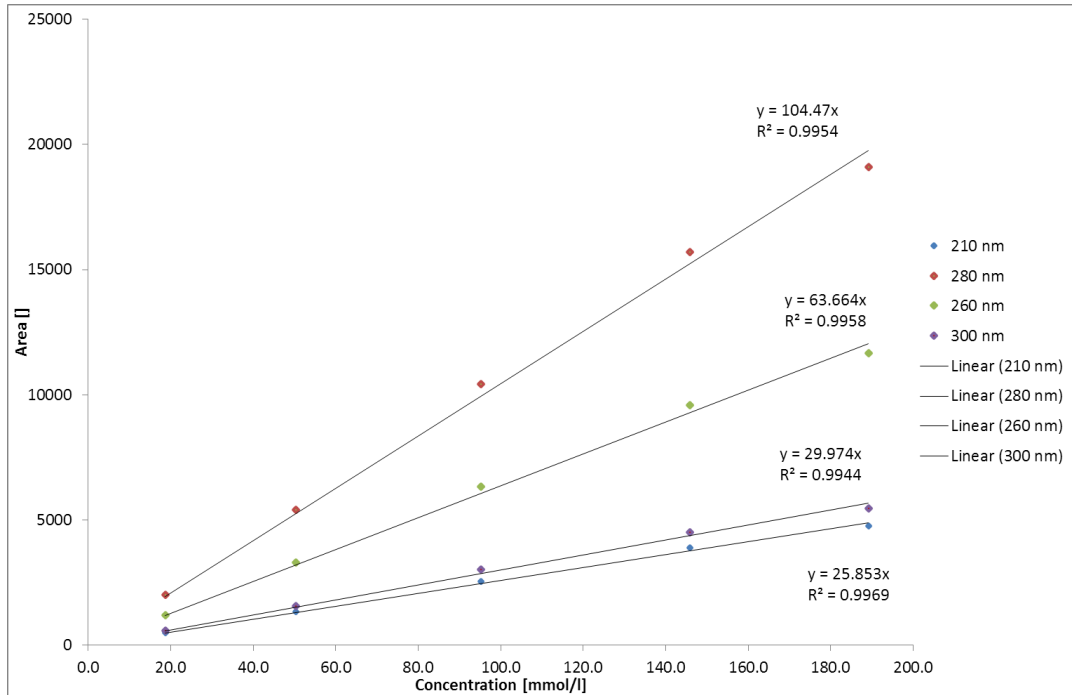


Figure 6.2: HPLC calibration of 7DHC. Area versus concentration

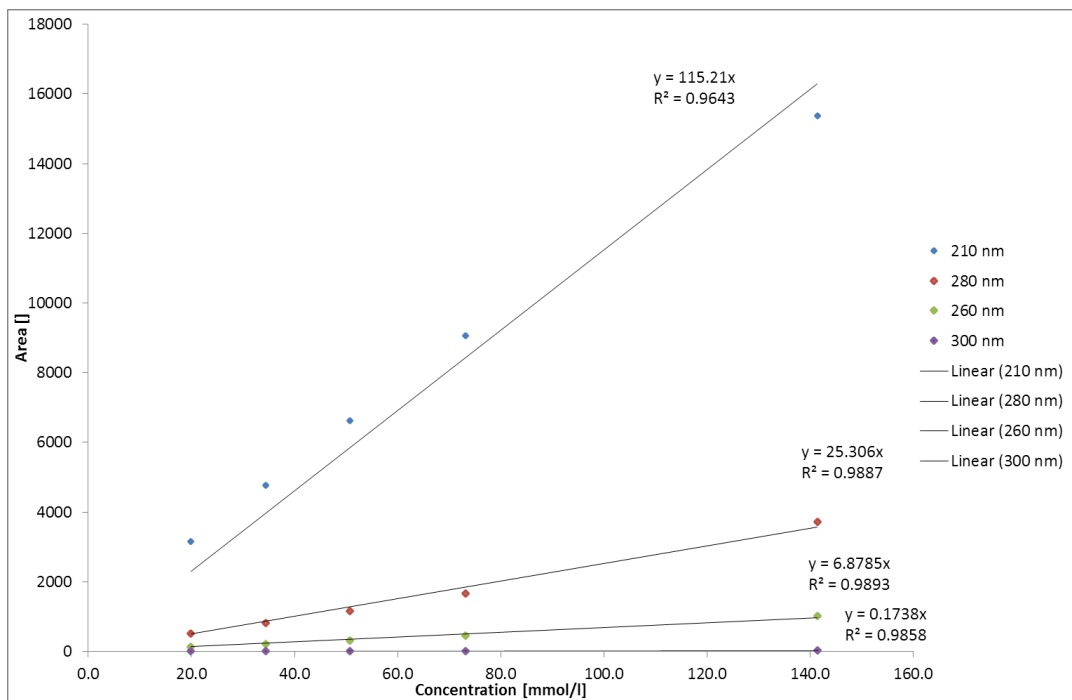


Figure 6.3: HPLC calibration of E321. Area versus concentration



## 6.2 Pumps

Two peristaltic pumps from ISMATEC® model ISM833C were used in this work. The tubing was a PharMed® MFG by SAINT-GOBAIN PPL. Calibration was done as described in the corresponding user manual.

## 6.3 Magnetic stirrer

For temperatures above 25°C the heatable magnetic stirrer C-MAG HS7 from IKA® was used.

## 6.4 Ultrasonic bath

The used ultrasonic bath was an Elma® Transsonic T780.

## 6.5 Thermostat - Heater/Cooler

Experiments with temperatures below 25°C were cooled with the thermostat LAUDA® alpha RA 12. It was used to cool the ultrasonic bath through a copper spiral attached to the external ports of the bath with tubes.

## 6.6 Vacuum pump and rotary evaporator

Evaporation of solvents was done in round bottom flasks attached to a rotary evaporator from Heidolph LABOROTA 4000 - efficient. The vacuum was applied by a vacuum pump unit PC 520 from vacuumbrand.

## 6.7 Microscope

Microscope pictures were taken using a Leica DM4000M microscope with an integrated digital camera.

## 6.8 Helos

Particle size distributions were measured as suspension in water using Tween20® as surfactant with a HELOS/KR Laser diffraction sensor equipped with a CUVETTE wet dispersion system by Sympatec GmbH (Cuvette Size: 50 ml, stirring speed 1000 rpm, optical concentration 1% - 20%, measuring range: combined R2+R5 (0.45  $\mu\text{m}$  - 875  $\mu\text{m}$ ), evaluation mode: Fraunhofer approximation, software: WINDOX 5.6.0.0).

## 6.9 Raman

Raman data was obtained using a Perkin Elmer Raman Station 400F. Exposure time: 1s, number of exposures: 10, sampling SuperMacropoint (7 points), wave length range: 200 3278  $\text{cm}^{-1}$ , Interval 2  $\text{cm}^{-1}$

## 6.10 Sampling from suspensions

The syringe filters Rotabilo<sup>®</sup> CA 0.2  $\mu\text{m}$  pore size and 25 mm membrane were used during the sampling from suspension to obtain a crystal free filtrate for the HPLC analysis.

## 6.11 Used chemicals

Compound	Abbr.	Notes	Product No.	Company
Acetonitrile	$\text{C}_2\text{H}_3\text{N}$	$\geq 99.9\%$	HN44.3	Carl Roth
tert-butyl methyl ether	$\text{C}_5\text{H}_{12}\text{O}$	$\geq 99.0\%$	20257-1L-F	Fluka
Vitamin D3	$\text{C}_{27}\text{H}_{44}\text{O}$	99.0%	D22524	Alfa Aesar
7-Dehydrocholesterol	$\text{C}_{27}\text{H}_{44}\text{O}$	$\geq 95\%$	BCBR2762V	Sigma-Aldrich
Acetic acid ethyl ester	$\text{C}_4\text{H}_8\text{O}_2$	$\geq 99.5\%$	7338.3	Carl Roth
Sodium chloride	NaCl	$> 99.8\%$	9265.2	Carl Roth
Butylated hydroxytoluene	E321	99.8%	219830500	Acros
Water	$\text{H}_2\text{O}$	deionized		

# 7 Appendix

## 7.1 Glossary

USP - United states pharmacopoeia

PSD - Particle size distributions

CSD - Crystal size distributions

VD3 - Vitamin D<sub>3</sub>

HPLC - High pressure liquid chromatography

7DHC - 7-Dehydrocholesterol

ACN - Acetonitrile

tBME - tert-Butyl methyl ether

E321 - Butylated hydroxytoluene

MSMPR - Mixed suspension mixed product removal crystallizer

OP - Operating point

# Bibliography

- [1] M. F. Holick, “The vitamin d epidemic and its health consequences,” *The Journal of nutrition*, vol. 135, no. 11, pp. 2739S–2748S, 2005.
- [2] N. Rodríguez-hornedo and D. Murphy, “Significance of controlling crystallization mechanisms and kinetics in pharmaceutical systems,” *Journal of pharmaceutical sciences*, vol. 88, no. 7, pp. 651–660, 1999.
- [3] A. Windans and F. Bock, “Über das provitamin aus dem sterin der schweineschwarte.,” *Hoppe-Seyler’s Zeitschrift für physiologische Chemie*, vol. 245, no. 3-4, pp. 168–170, 1936.
- [4] M. M. Eliot, E. Nelson, D. J. Barnes, F. A. Browne, and R. M. Jenss, “A study of the comparative value of cod liver oil, viosterol, and vitamin d milks in the prevention of rickets and of certain basic factors influencing their efficacy,” *The Journal of Pediatrics*, vol. 9, no. 3, pp. 355–376, 1936.
- [5] A. L. Hirsch, “Industrial aspects of vitamin d,” in *Chapter 6 in Vitamin D: Two-Volume Set*, pp. 73–93, Academic Press, 2011.
- [6] A. Windans and F. Schenck, “Dehydro-sterol compounds and manufacture thereof,” Nov. 16 1937. US Patent 2,098,984.
- [7] A. Windans and F. Schenck, “Antirachitic vitamin,” Nov. 16 1937. US Patent 2,099,550.
- [8] T. Tan and L. Zhang, “Preparation method for 7-dehydrochol esterol,” July 16 2008. CN Patent App. CN 200,810,056,886.
- [9] J. Can, S. Weike, W. Guangdong, W. Ziqinag, and M. Huanzheng, “Chemical synthesis method of 5,7-diene steroids compounds,” May 25 2011. CN Patent 101,381,389.
- [10] M. Braun, W. Fuss, K. Kompa, and J. Wolfrum, “Improved photosynthesis of previtamin d by wavelengths of 280–300 nm,” *Journal of Photochemistry and Photobiology A: Chemistry*, vol. 61, no. 1, pp. 15–26, 1991.
- [11] M. Escribà-Gelonch et al., “Presentation,” *ProcessNet Jahrestagung*, 2016.
- [12] J.-R. Wang, B. Zhu, Q. Yu, and X. Mei, “Selective crystallization of vitamin d 3 for the preparation of novel conformational polymorphs with distinctive chemical stability,” *CrystEngComm*, vol. 18, no. 7, pp. 1101–1104, 2016.

- [13] H. J. Jacobs, "Photochemistry of conjugated trienes: Vitamin d revisited," *Pure and applied chemistry*, vol. 67, no. 1, pp. 63–70, 1995.
- [14] R. M. Wing, W. H. Okamura, M. R. Pirio, S. M. Sine, and A. W. Norman, "Vitamin d in solution: conformations of vitamin d<sub>3</sub>, 1 $\alpha$ , 25-dihydroxyvitamin d<sub>3</sub> and dihydrotachysterol<sub>3</sub>," *Science*, vol. 186, no. 4167, pp. 939–941, 1974.
- [15] R. M. Wing, W. H. Okamura, A. Rego, M. R. Pirio, and A. W. Norman, "Vitamin d and its analogs. vii. solution conformations of vitamin d<sub>3</sub> and 1. alpha., 25-dihydroxyvitamin d<sub>3</sub> by high-resolution proton magnetic resonance spectroscopy," *Journal of the American Chemical Society*, vol. 97, no. 17, pp. 4980–4985, 1975.
- [16] H. Gruber-Woelfler, M. Escribà-Gelonch, T. Noël, M. C. Maier, and V. Hessel, "Effect of acetonitrile-based crystallization conditions on the crystal quality of vitamin D<sub>3</sub>," *ChemEngTech*, 2017.
- [17] H. Klein, K. Schaaf, and S. Seymour, "Process for obtaining purified crystalline vitamin d," Aug. 1 1967. US Patent 3,334,118.
- [18] R. Marbet, "Process for the preparation of crystalline vitamin d<sub>3</sub>," May 23 1972. US Patent 3,665,020.
- [19] R. Reintjens and A. Puhl, "Photochemical process for the preparation of a previtamin d," Oct. 30 2008. WO Patent App. PCT/EP2008/003,321.
- [20] G. Hofmann, *Kristallisation in der industriellen Praxis*. John Wiley & Sons, 2004.
- [21] J. Gibbs, *The Collected Works. Vol. 1. Thermodynamics*. Yale University Press, 1948.
- [22] J. Mullin, "5 - nucleation," in *Crystallization (Fourth Edition)* (J. Mullin, ed.), pp. 181 – 215, Oxford: Butterworth-Heinemann, fourth edition ed., 2001.
- [23] M. Volmer, "Kinetik der phasenbildung, steinkopff," *Leipzig, Germany*, 1939.
- [24] R. Becker and W. Döring, "Kinetische behandlung der keimbildung in übersättigten dämpfen," *Annalen der Physik*, vol. 416, no. 8, pp. 719–752, 1935.
- [25] A. Ranodolph, *Theory of particulate processes: analysis and techniques of continuous crystallization*. Elsevier, 2012.
- [26] K. Berglund, "4 - analysis and measurement of crystallization utilizing the population balance," in *Handbook of Industrial Crystallization (Second Edition)* (A. S. Myerson, ed.), pp. 101 – 113, Woburn: Butterworth-Heinemann, second edition ed., 2002.
- [27] R. Liang, Z. Bao, B. Su, H. Xing, and Q. Ren, "Solubility of vitamin d<sub>3</sub> in six organic solvents at temperatures from (248.2 to 273.2) k," *Journal of Chemical & Engineering Data*, vol. 57, no. 8, pp. 2328–2331, 2012.

- [28] J.-R. Wang, Q. Yu, W. Dai, and X. Mei, “Drug–drug co-crystallization presents a new opportunity for the development of stable vitamins,” *Chemical Communications*, vol. 52, no. 17, pp. 3572–3575, 2016.